# Prospects of detecting deviations to Kerr geometry with radiation reaction effects in EMRIs

Abhishek Chowdhuri<sup>1</sup>, Arpan Bhattacharyya<sup>2</sup> and Shailesh Kumar<sup>3</sup>

Indian Institute of Technology, Gandhinagar, Gujarat-382355, India

#### ABSTRACT

Direct detection of gravitational waves and binary black hole mergers have proven to be remarkable investigations of general relativity. In order to have a definitive answer as to whether the black hole spacetime under test is the Kerr or non-Kerr, one requires accurate mapping of the metric. Since EMRIs are perfect candidates for space-based detectors, Laser Interferometer Space Antenna (LISA) observations will serve a crucial purpose in mapping the spacetime metric. In this article, we consider such a study with the Johannsen spacetime that captures the deviations from the Kerr black hole and further discuss their detection prospects. We analytically derive the leading order post-Newtonian corrections in the average loss of energy and angular momentum fluxes generated by a stellar-mass object exhibiting eccentric equatorial motion in the Johannsen background. We further study the orbital evolution of the inspiralling object within the adiabatic approximation. We lastly provide the possible detectability of deviations from the Kerr black hole by estimating gravitational wave dephasing and highlight the crucial role of LISA observations.

<sup>&</sup>lt;sup>1</sup>chowdhuri\_abhishek@iitgn.ac.in

 $<sup>^2</sup>$ abhattacharyya@iitgn.ac.in

<sup>&</sup>lt;sup>3</sup>shailesh.k@iitgn.ac.in

### Contents

1	Introduction	1
2	Deformed Kerr geometry: An introduction	4
3	Geodesic motion and eccentric orbital dynamics	6
4	Radiation reaction: GW fluxes and orbital evolution	8
5	Detection prospects with GW dephasing	15
6	Discussion	18
A	Geodesic velocities and constants of motion	20
$\mathbf{B}$	Orbital evolution	22

#### 1 Introduction

The series of detections by LIGO and Virgo collaborations [1–7] for gravitational waves (GWs) has opened up opportunities for new insights into the cosmos. GW astronomy is now a critical tool for answering longstanding non-trivial questions on astronomy and cosmology and offers a test of gravity in a strong and weak regime. The detectors boast a high level of precision, which will only improve in the years to come, thus demanding commensurately accurate theoretical predictions encoded in waveform templates, which will be utilized for detection and parameter estimations. These waveforms are constructed from various techniques, including the effective one-body (EOB) formalism [8,9], numerical relativity [10–12], self-force techniques [13,14], and several perturbative methods for the inspiral phase, including the post-Newtonian (PN) [15,16] and post-Minkowskian (PM) approximations [17,18], as well as effective field theory (EFT) formalisms [19–23]. Further improving these high-precision theoretical predictions from general relativity (GR) or other alternate gravity theories (non-GR) will be crucial, given the expected sensitivity improvements in the detectors.

Here, we will focus on one of the above techniques, which has time and again proved to be a useful theoretical tool for building waveforms: the PN scheme. During the early inspiral phase, where the gravitational system is weak, the constituents of the binary black hole systems can be treated as non-relativistic, and one can impose an expansion in velocity squared which is of the order of inverse separation in units of the Schwarzschild radius due to the virial theorem. This expansion has a well-established framework with a long history dating back to the leading 1PN correction to the Newtonian gravitational potential [15] with follow-up works on 2PN [24], 3PN [25–28], and

4PN [29–37] expressions for the conservative potential. More recently, 5PN static contributions have also been computed [38, 39]. Apart from such analyses happening for GR, much work has been done in extending this PN scheme for non-GR theories as well [40–43]. The formalism can also be extended for hyperbolic encounters [44–46], for binaries moving in media [47, 48], in the context of EFTs using the worldline EFT approaches [49–54]. In this paper, we will only focus on the leading order term in this expansion, giving us the leading order contribution in the energy flux for binaries.

While it is sufficient for weak-field regime analysis to rely on the PN approach, a model-independent strong-field test requires an underlying spacetime geometry. The most obvious one that is used is a deformed Kerr metric, with the deviations being parametric. Several such frameworks have been suggested within which possible observational signatures of a Kerr-like black hole can be explored [55–58]. As these deviations are parametric, it follows that the observables obtained for these metrics should depend on one or more of these parameters. They have a smooth Kerr limit when the deviations vanish. These metrics can prove to be useful in validating GR. Further, in view of testing the "no-hair" theorems, these theories along with deviations have been studied in the strong field regime [59], with the obvious expectation that it aligns with the weak field tests [60]. A deviation from the Kerr metric puts forward two possible interpretations. Within GR, the object, described by this kind of geometry, cannot be a black hole but instead can be a stable stellar or an exotic object [55,61].

However, such deformations do introduce some pathologies as well [61]. In GR, the "no-hair" theorem guarantees the "Kerr Metric" is the only possible vacuum solution with two independent parameters: mass and spin. So, any deviation from this geometry will naturally violate the assumptions of this theorem, and this is exactly the reason that it might lead to situations such as the existence of closed time-like curves, null singularities, etc., hampering useful analysis in the strong field regime. In [61], authors analyze such parametric deviations in detail and explicitly show how they differ from the Kerr metric. Identifying the regions where these parameters are unphysical and the range of coordinates and parameters for which each extension remains regular is a possible way to circumvent these pathologies. Such a dependence is enough to test the no-hair theorem as long as these deviations are small. Large deviations, in turn, require understanding the strong-field radiative dynamics in the theory. To understand strong-field physics, one generally does not require the dynamical properties of the gravity theory and the underlying field equations. In most of the tests of strong field regime, one can generally find out that tests of the no-hair theorem in the electromagnetic spectrum [62–69], however, they are not a priori limited to the study of small deviations from the Kerr metric because these are performed in a stationary black hole spacetime, where the metric serves as a fixed background.

Several model-independent strong-field tests of the no-hair theorem have been suggested using GW observations of extreme mass ratio inspirals (EMRIs) [70–74], where an object (secondary with

mass  $\mu$ ) inspirals the central supermassive black hole (primary with mass M). Hence, exploring waveforms in this context can be a useful tool. As the name suggests, such binaries have a mass ratio lying in the range ( $q \equiv \mu/M = 10^{-7} - 10^{-4}$ ) and radiate GWs in the millihertz range, making it one of the most sought-after objects in LISA [75]. Much work has been done to look for theoretically modelling such signals [76–88] in the hope that they will infer the dynamics of the compact object deep in the gravitational field of the central black hole. It allows us to probe intergalactic astrophysical environment [89] and also place constraints for both modelling and data analysis of EMRIs.

Focusing our attention to the part of the parameter space where we can evade pathologies, we examine the effects of gravitational radiation reaction on orbits moving in the deformed Kerr geometry. In [90], these deformations in the context of Manko-Novikov type metrics have been studied to understand resonant glitches. We do our analysis by keeping only the leading order contribution coming due to the deviation parameters which enter in the expressions for various fluxes at 2PN order and to the leading order in mass ratio. We also assume adiabatic approximation, meaning the radiation reaction timescale is much longer than the orbital period; thus, the orbit looks geodesic on shorter timescales. The analysis we follow is similar to the one in [70,91], where we use the leading order radiation reaction acceleration that acts on the particle. We keep the parameter responsible for axisymmetry breaking to analyse the effects it has on the phasing and dephasing of the gravitational waves<sup>4</sup>. In the adiabatic limit, the time-averaged rates governing the change in the constants of motion help us infer the orbital evolution.

Before concluding, let us go through how we organize the paper: After a brief introduction on deformed geometries in Section (2), we discuss the geodesic motions of the particle in such geometry in Section (3). This gives us an idea of the orbital dynamics of the inspiralling object. Next, in Section (4), we introduce the radiation reaction formalism and discuss the changes in the orbital parameters. Section (5) is solely focused on exploring the detection possibilities for our setup, where we go on to calculate dephasing. We conclude by discussing our results in Section (6) with possible future directions. Some additional details are given in the appendices (A) and (B).

Notation and Convention: We set the fundamental constants G and c to unity and adopt positive sign convention (-1,1,1,1). Roman letters are used to denote spatial indices, and Greek letters are used to represent four-dimensional indices.

<sup>&</sup>lt;sup>4</sup>This analysis is much different from the one in [86] where they have analysed scenarios for equatorial symmetry breaking for Kerr metric and their associated analytic Kludge waveforms.

# 2 Deformed Kerr geometry: An introduction

We begin by considering the usual Kerr metric describing a rotating black hole spacetime. The line element is well-known and given by

$$ds^{2} = -\sum \frac{\Delta - a^{2} \sin^{2} \theta}{N} dt^{2} + \sum \frac{\Delta}{\Delta} dr^{2} + \sum d\theta^{2} - 2a \sum \sin^{2} \theta \frac{(r^{2} + a^{2}) - \Delta}{N} dt d\phi +$$

$$\sum \sin^{2} \theta \frac{(r^{2} + a^{2})^{2} - a^{2} \Delta \sin^{2} \theta}{N} d\phi^{2},$$
(2.1)

where  $\Sigma \equiv r^2 + a^2 \cos^2 \theta$ ,  $\Delta \equiv r^2 - 2Mr + a^2$  and  $N \equiv \Sigma^2$ . The above metric is Petrov Type D and admits a third constant of motion, the Carter constant  $\mathcal{Q}$  apart from the energy E, and the axial angular momentum  $J_z$ . The Carter constant  $\mathcal{Q}$  is then introduced while solving the Hamilton-Jacobi equation by the standard method, which assumes that it is separable. The equation reads like

$$g^{\alpha\beta} \frac{\partial}{\partial x^{\alpha}} \frac{\partial}{\partial x^{\beta}} = -\frac{1}{\Delta \Sigma} \left[ -(r^2 + a^2)E + aJ_z \right]^2 + \frac{1}{\Sigma \sin^2 \theta} \left[ J_z - aE \sin^2 \theta \right]^2 + \frac{\Delta}{\Sigma} \left( \frac{\partial S_r}{\partial r} \right)^2 + \frac{1}{\Sigma} \left( \frac{\partial S_\theta}{\partial \theta} \right)^2$$
(2.2)

where  $S_r$  and  $S_\theta$  are the radial and angular parts of the Hamilton-Jacobi function; see Eq.(A.1). Upon rearranging the terms, we can write down two separate equations for the radial and angular parts and, in principle, solve them. However, Johannsen in [92] explored the idea of introducing deviations to Kerr metric such that the Hamilton-Jacobi still admits separability. After introducing scalar functions like f(r), g(r),  $A_i(r)$  with i = 1, 2, 5, and  $A_j(\theta)$  with j = 3, 4, 6, the Hamilton-Jacobi equation takes the following form:

$$g^{\alpha\beta} \frac{\partial}{\partial x^{\alpha}} \frac{\partial}{\partial x^{\beta}} = -\frac{1}{\Delta \tilde{\Sigma}} \left[ (r^{2} + a^{2}) A_{1}(r) \frac{\partial}{\partial t} + a A_{2}(r) \frac{\partial}{\partial \phi} \right]^{2} + \frac{1}{\tilde{\Sigma} \sin^{2} \theta} \left[ A_{3}(\theta) \frac{\partial}{\partial \phi} + a A_{4}(\theta) \sin^{2} \theta \frac{\partial}{\partial t} \right]^{2} + \frac{\Delta}{\tilde{\Sigma}} A_{5}(r) \left( \frac{\partial}{\partial r} \right)^{2} + \frac{1}{\tilde{\Sigma}} A_{6}(\theta) \left( \frac{\partial}{\partial \theta} \right)^{2}$$

$$(2.3)$$

where  $\tilde{\Sigma} = \Sigma + f(r) + g(\theta)$  [92]. Then similar to the Kerr case, one can come up with an equivalent expression to Eq.(2.2):

$$g^{\alpha\beta} \frac{\partial}{\partial x^{\alpha}} \frac{\partial}{\partial x^{\beta}} = -\frac{1}{\Delta \tilde{\Sigma}} [-(r^2 + a^2)A_1(r)E + aA_2(r)J_z]^2 + \frac{1}{\tilde{\Sigma}\sin^2\theta} [A_3(\theta)J_z - aA_4(\theta)E\sin^2\theta]^2 + \frac{\Delta}{\tilde{\Sigma}} A_5(r) \left(\frac{\partial S_r}{\partial r}\right)^2 + \frac{1}{\tilde{\Sigma}} A_6(\theta) \left(\frac{\partial S_\theta}{\partial \theta}\right)^2.$$
(2.4)

The point of writing the above equation is to show that even after introducing some r and  $\theta$  dependent deviation functions, one can still separate the equations and show the existence of a Carter-like constant.  $\tilde{\Sigma}$  is a function of r and  $\theta$  both. One can easily read off contravariant and covariant forms of the metric and impose further conditions to constrain the form of the above deviation functions in the following way [92]: regularity of the metric gives  $A_5(r) > 0$ , the conditions for asymptotic flatness gives  $A_6(\theta) = 1$ . Also, one can expand the deviation functions in powers of  $\frac{M}{r}$  with coefficients of each term given by  $\alpha_{i,n}$  where  $i = 1, \dots, n$  denoting the power of  $\frac{M}{r}$  and  $n = 1, \dots, 5$  denote the deviation functions. If one expands the metric in  $\frac{1}{r}$ ,  $A_3(\theta)$ ,  $A_4(\theta)$  get constrained to 1 [92]. The deviation parameters can also be further constrained using PPN constraints<sup>5</sup>. Summarizing all of these and keeping only the next-to-leading order term in the metric expansion, the metrics take the following form [92, 93]:

$$ds^{2} = -\tilde{\Sigma} \frac{\Delta - a^{2} A_{2}^{2} \sin^{2} \theta}{N} dt^{2} + \frac{\tilde{\Sigma}}{\Delta A_{5}} dr^{2} + \tilde{\Sigma} d\theta^{2} - 2a\tilde{\Sigma} \sin^{2} \theta \frac{(r^{2} + a^{2}) A_{1} A_{2} - \Delta}{N} dt d\phi + \qquad (2.5)$$

$$\tilde{\Sigma} \sin^{2} \theta \frac{(r^{2} + a^{2})^{2} A_{1}^{2} - a^{2} \Delta \sin^{2} \theta}{N} d\phi^{2},$$

where  $A_1, A_2, A_5$  and N are functions of radial coordinate r, given by

$$A_{1}(r) = 1 + \alpha_{13} \left(\frac{M}{r}\right)^{3} ; \qquad N(r) = \left((r^{2} + a^{2})A_{1} - a^{2}A_{2}\sin^{2}\theta\right)^{2},$$

$$A_{2}(r) = 1 + \alpha_{22} \left(\frac{M}{r}\right)^{2} ; \qquad \Delta(r) = r^{2} - 2Mr + a^{2},$$

$$A_{5}(r) = 1 + \alpha_{52} \left(\frac{M}{r}\right)^{2} ; \qquad \tilde{\Sigma} = r^{2} + a^{2}\cos^{2}\theta + \epsilon_{3}\frac{M^{3}}{r}, \qquad (2.6)$$

where  $(\alpha_{13}, \alpha_{22}, \alpha_{52}, \epsilon_3)$  denote deformation parameters in Kerr. The interesting point about this metric is that the event horizon and the multipole moments coincide with that of the Kerr.

Note that, following [62–65,92,94], we have applied constraints coming from parametrized-post-Newtonian (ppN) framework. Otherwise, we have to deal with more deviation parameters.<sup>6</sup>. Even after using such constraints, the parameters  $\alpha_{i,n}s$  as indicated in Eq.(2.6) remain unconstrained. One may, in principle, consider large numerical values for these parameters. However, since we perform all our analysis in this paper perturbatively for deviation parameters, assuming that the dominant contribution always comes from GR, we keep them small and consider only corresponding leading-order PN contributions.

<sup>&</sup>lt;sup>5</sup>The reader is encouraged to look into [92] for further details.

<sup>&</sup>lt;sup>6</sup>It should be noted that the ppN constraints are obtained assuming the central object is a star. Therefore, to apply these constraints, we must further assume that the asymptotic behaviours of metric components for a star and a black hole geometry are the same [94,95].

# 3 Geodesic motion and eccentric orbital dynamics

In this section we discuss the leading order effects of Johannsen parameters (deviation parameters to the Kerr) as defined in Eq.(2.6) on the eccentric equatorial orbital motion of the inspiralling object. Since, the metric has two Killing vectors  $(\partial_t)^{\mu}$  and  $(\partial_{\phi})^{\mu}$ , it gives rise to two conserved quantities energy (E) and angular momentum  $(J_z)$ . We also have the third constant of motion, the Carter constant. Since we focus on equatorial motion  $(\theta = \pi/2)$ , the Carter constant will be zero (Q = 0) [96–98]. It is always good to introduce dimensionless quantities:  $\hat{r} = r/M$ ,  $\hat{a} = a/M$ ,  $\hat{J}_z = J_z/(\mu M)$  and  $\hat{E} = E/\mu$ ; We will further set M = 1. For writing convenience, we avoid putting the hat over the aforesaid quantities. With this, the equations of motion of the object upto  $\mathcal{O}(a)$  can be written in the following way

$$\frac{dt}{d\tau} = \left[ -(r^2 A_1 A_2 - \Delta) \frac{aJ_z}{r^2 \Delta} + \frac{Er^2}{\Delta} A_1^2 \right] \left( 1 + \frac{\epsilon_3}{r^3} \right)^{-1} + \mathcal{O}(a^2)$$

$$\frac{d\phi}{d\tau} = \left[ \frac{J_z}{r^2 \sin^2 \theta} + \frac{aE}{r^2 \Delta} (A_1 A_2 r^2 - \Delta) \right] \left( 1 + \frac{\epsilon_3}{r^3} \right)^{-1} + \mathcal{O}(a^2)$$

$$\left( \frac{dr}{d\tau} \right)^2 = \frac{A_5}{\Sigma^2} \left[ (A_1 r^2 E - aA_2 J_z)^2 - \Delta \left( Q + r^2 + \frac{\epsilon_3}{r} \right) \right] + \mathcal{O}(a^2)$$

$$\left( \frac{d\theta}{d\tau} \right)^2 = \frac{1}{\Sigma^2} \left[ Q - \left( aE \sin \theta - \frac{J_z}{\sin \theta} \right)^2 \right] + \mathcal{O}(a^2),$$
(3.1)

where,  $Q \equiv Q - (J_z - aE)^2$ . Since Q = 0, it implies that  $Q = J_z^2 - 2aEJ_z + \mathcal{O}(a^2)$  as also discussed in appendix (A). We further analyze the radial equation in Eq.(3.1), which governs the object's orbital motion and provides us with the effective potential  $(V_{eff})$ . In general, without loss of generality, one can also express the effective potential for equatorial orbits in terms of metric coefficients as [89]

$$\left(\frac{dr}{d\tau}\right)^2 = -V_{eff}(r), \text{ where, } V_{eff}(r) = \frac{1}{2}(g^{tt}E^2 - 2g^{t\phi}EJ_z + g^{\phi\phi}J_z^2 + 1).$$
 (3.2)

Note that we keep only upto leading order terms in spin and Johannsen parameters  $(a, \alpha_{13}, \alpha_{52}, \alpha_{22}, \epsilon_3)$  and discard subleading corrections.

As we aim to examine the eccentric dynamics of the object, we take two turning points  $(r_a, r_p)$  for bound orbits where the radial velocity vanish  $(V_{eff} = 0)$ , denoting apastron and periastron respectively. The bound orbits can be written in terms of eccentricity (e) and semi-latus rectum (p) as

$$r_a = \frac{p}{1-e}$$
 ;  $r_p = \frac{p}{1+e}$ . (3.3)

The condition for bound orbits in the range  $r_p < r < r_a$  is  $V_{eff}(r) < 0$ , which is satisfied only when  $V'_{eff}(r_a) > 0$  and  $V'_{eff}(r_p) \le 0$  [99]; where, prime denotes the derivative with respect to r. Using Eq.(3.2) and Eq.(3.3), at the turning points for the system under consideration, one can derive the

constants of motion of the bound orbits; the positive roots of  $(E, J_z)$  read as

$$E = \sqrt{\frac{(p-2)^2 - 4e^2}{p(p-3-e^2)}} + \frac{(e^2 - 1)^2}{p(p-3-e^2)^{3/2}} \left[ -a + \frac{\alpha_{13}\sqrt{(p-2)^2 - 4e^2}}{2p^{3/2}} \right] - \frac{\epsilon_3(e^2 - 1)^2}{4} \sqrt{\frac{(p-2)^2 - 4e^2}{p^7(p-3-e^2)}},$$
(3.4)

$$J_z = \frac{p}{\sqrt{p-3-e^2}} + (3+e^2)\sqrt{\frac{(p-2)^2 - 4e^2}{p(p-3-e^2)^3}} \left[ -a + \frac{\alpha_{13}\sqrt{(p-2)^2 - 4e^2}}{2p^{3/2}} \right] - \frac{\epsilon_3 \left( e^2(p-8) + 3p - 8 \right)}{4p^2\sqrt{p-3-e^2}}.$$
(3.5)

We remind that we only consider leading order corrections in spin and Johannsen parameters through out the article. Once we have the constants of motion, one can always determine the last stable orbit (LSO) of the inspiralling object [96,100]. This requires the following condition to satisfy:  $V_{eff}(r_p) = 0$ ,  $V_{eff}(r_a) = 0$ ;  $V'_{eff}(r_p) = 0$ ,  $V'_{eff}(r_a) > 0$ . From Eqs.(3.2, 3.3, 3.4, 3.5), one can obtain the set of (p, e) points that will separate the bound orbits from unbounded ones [101, 102]. We term such a region as *separatrix*, and the expression takes the following form

$$p_{sp} = 2(e+3) - 4\sqrt{2}a\sqrt{\frac{e+1}{e+3}} + 4\alpha_{13}\frac{(e+1)}{(e+3)^2} - \epsilon_3\frac{(e-3)^2(e+1)^2}{4(e+3)^3}.$$
 (3.6)

To put it another way, the separatrix determines the lowest semi-latus rectum value for which spacetime permits bound orbits for a given eccentricity. It is the last stable orbit of the motion. For circular orbits (e = 0), it is called the innermost stable circular orbit (ISCO). The Eq.(3.6) corresponds to the prograde motion of the inspiralling object and coincides with [97] in leading order a; however, one can replace  $a \to -a$  for the retrograde motion. It implies that the separatrix curve for prograde (retrograde) orbits will shift to the left (right) with respect to the Schwarzschild curve  $(p_{sp}^{sch} = 6 + 2e)$  as the black hole spins up [97].

The motion occurs between  $r_p$  to  $r_a$  and vice-versa. As we choose r as the parameter throughout the orbit, we can integrate Eq.(3.1) by removing  $\tau$  from the set of equations. We parametrize the radial coordinate r in the following way to conquer the divergences at the turning points  $(V_{eff} = 0; r_a, r_p)$ 

$$r = \frac{p}{1 + e\cos\gamma} \,. \tag{3.7}$$

This parametrization helps in removing the singular behaviour at the turning points  $(r_a, r_p)$  in the differential equations, i.e., in geodesic velocities, implying  $(\chi = \pi, \chi = 0)$  respectively. Further, the eccentric motion exhibits two fundamental frequencies: radial  $(\Omega_{\phi})$  and azimuthal  $(\Omega_r)$ . It has been shown that the radial motion shows the periodicity, not the azimuthal one [101]; hence, using

Eq.(3.1),  $(\Omega_{\phi}, \Omega_r)$  are given by

$$\Omega_{\phi} = \frac{1}{Er^{3}} \left( J_{z}(r-2) + \frac{a \left( 2E^{2}r^{3} + 2J_{z}^{2}(r-2) \right)}{Er^{3}} - \frac{2\alpha_{13}J_{z}(r-2)}{r^{3}} \right), 
\Omega_{r} = \frac{2\pi}{T_{r}} ; \quad T_{r} = \int_{0}^{2\pi} d\chi \frac{dt}{d\chi} ; \quad \frac{dt}{d\chi} = \frac{dt}{dr} \frac{dr}{d\chi}.$$
(3.8)

In general,  $\Omega_{\phi}$  can be written in terms of metric coefficients:  $\Omega_{\phi} = -\frac{g_{t\phi}E + g_{tt}J_z}{g_{\phi\phi}E + g_{t\phi}J_z}$ , that coincides in linear order corrections with [94].  $T_r$  is the radial time period. We use these relevant quantities later in subsequent sections for estimating fluxes.

## 4 Radiation reaction: GW fluxes and orbital evolution

Let us turn our discussion to the GW radiation reaction acceleration or force that gradually alters the orbital dynamics of the inspiralling object. As we consider an EMRI system, the primary supermassive black hole is being perturbed by the secondary object that plays the role of a test particle. As a result, emitted GWs introduce the notion of GW radiation reaction, which infers that the constants of motion no longer remain constants; they start evolving in time. Although the overall scenario necessitates a complete numerical analysis [103], we analyze effects within the leading order PN corrections as well as leading order in the mass ratio. We mainly follow the analysis of [70,91,104]. In this section, we provide a general setup to estimate the average energy and angular momentum fluxes due to the radiation reaction effects for eccentric equatorial orbits and examine the leading order deviations from the Kerr results.

It is useful to introduce Cartesian coordinates  $(x_1, x_2, x_3) = (r \sin \theta \cos \phi, r \sin \theta \sin \phi, r \cos \theta)$  for expressing the constants of motion and their change. The conserved quantities in the leading order of deviation parameters have been derived in Eqs.(A.16, A.20, A.22) and are given in Cartesian coordinates as

$$\mathcal{E} = \frac{1}{2}\dot{x}_i\dot{x}_i - \frac{1}{\sqrt{x_i x_i}},\tag{4.1}$$

$$J_z = \epsilon_{3jk} x_j \dot{x}_k \left( 1 + \frac{\epsilon_3}{(x_i x_i)^{3/2}} \right) - 2a \frac{(x_1^2 + x_2^2)}{(x_i x_i)^{3/2}}, \tag{4.2}$$

$$Q + J_z^2 = (\epsilon_{ijk} x_j \dot{x}_k) (\epsilon_{ilm} x_l \dot{x}_m) - 4a \frac{\epsilon_{3jk} x_j \dot{x}_k}{\sqrt{x_i x_i}}, \tag{4.3}$$

where  $r^2 \sin^2 \theta \dot{\phi} = \epsilon_{3jk} x_j \dot{x}_k$  and  $r^4 (\dot{\theta}^2 + \sin^2 \theta \dot{\phi}^2) = (\epsilon_{ijk} x_j \dot{x}_k) (\epsilon_{ilm} x_l \dot{x}_m)$ , and dot denotes the derivative with respect to coordinate time t. Note that the analysis explained here is also valid for non-equatorial orbits and will match with the results of [91] up to linear order in a. We will set  $\theta = \pi/2$  at a later stage while computing the average fluxes for the ease of the computation. The radiation reaction effect causes the perturbed system to generate instantaneous fluxes, i.e., the rate

change of constants of motion takes the following form

$$\dot{\mathcal{E}} = x_i \ddot{x}_i \; ; \; \dot{J}_z = \epsilon_{3jk} x_j \ddot{x}_k \left( 1 + \frac{\epsilon_3}{(x_i x_i)^{3/2}} \right) \; ; \; \dot{\mathcal{Q}} + (\dot{J}_z^2) = 2(\epsilon_{ijk} x_j \dot{x}_k) (\epsilon_{ilm} x_l \ddot{x}_m) - \frac{4a\epsilon_{3jk} x_j \ddot{x}_k}{\sqrt{x_i x_i}}.$$
(4.4)

Since we are interested in analyzing the contributions of the radiative part, we only consider terms involving acceleration, also called radiation reaction acceleration and often denoted by  $a_j$ . The general expression of the same is given as [91, 104]

$$a_{j} = -\frac{2}{5}I_{jk}^{(5)}x_{k} + \frac{16}{45}\epsilon_{jpq}J_{pk}^{(6)}x_{q}x_{k} + \frac{32}{45}\epsilon_{jpq}J_{pk}^{(5)}x_{k}\dot{x}_{q} + \frac{32}{45}\epsilon_{pq[j}J_{k]p}^{(5)}x_{q}\dot{x}_{k} + \frac{8J}{15}J_{3i}^{(5)}, \tag{4.5}$$

where  $I_{jk}$  and  $J_{jk}$  are termed as mass and current quadrupole moments. The last term with J is the spin parameter (a) of the central black hole. The superscripts define the order of derivative of a quantity. For the third term, the anti-symmetric quantity can written as  $B_{[ij]} = \frac{1}{2}(B_{ij} - B_{ji})$ . We take the symmetric trace-free (STF) part of the mass and current moments in the following manner

$$I_{jk} = \left[ x_j x_k \right]^{\text{STF}} \quad ; \quad J_{jk} = \left[ x_j \epsilon_{kpq} x_p \dot{x}_q - \frac{3}{2} x_j J \delta_{k3} \right]^{\text{STF}}. \tag{4.6}$$

We compute the quantities mentioned in Eq.(4.6) and replace them in the Eq.(4.5). Further, to estimate the instantaneous change of the constants of motion, we make use of Eq.(4.5) and Eq.(4.4). Since we focus on the equatorial orbital motion, the expression in Eq.(4.4) involving the Carter constant will not be considered for computing the evolution of constants of motion as  $\theta = \pi/2$ .

The radiation reaction force causes the constants of motion to evolve in time. We use velocities (A.17) and calculate these quantities, and further average them out. We perform that computation upto the leading order in  $(a, \alpha_{13}, \epsilon_3, \alpha_{52}, \alpha_{22})$ . This also sets up the platform to analyze the effects of Johannsen parameters in the orbital evolution of the inspiralling object. The instantaneous fluxes or rate change of constants of motion are given as

$$\begin{split} \dot{\mathcal{E}} &= \frac{272J_z^2\mathcal{E}}{5r^5} + \frac{160J_z^2}{3r^6} - \frac{40J_z^4}{r^7} + a\left(\frac{196J_z^5}{r^9} - \frac{3668J_z^3}{5r^8} - \frac{352J_z^3\mathcal{E}}{r^7} + \frac{952J_z}{3r^7} + \frac{1024J_z\mathcal{E}}{3r^6} + \frac{128J_z\mathcal{E}^2}{5r^5}\right) \\ &+ \alpha_{52}\left(\frac{2048J_z^6}{5r^{10}} - \frac{20192J_z^4}{15r^9} - \frac{4352J_z^4\mathcal{E}}{5r^8} + \frac{5696J_z^2}{5r^8} + \frac{19504J_z^2\mathcal{E}}{15r^7} + \frac{256J_z^2\mathcal{E}^2}{r^6} - \frac{320}{3r^7} - \frac{1216\mathcal{E}}{5r^6} - \frac{128\mathcal{E}^2}{r^5}\right) \\ &+ \alpha_{13}\left(-\frac{392J_z^4}{r^9} + \frac{4256J_z^2}{5r^8} + \frac{752J_z^2\mathcal{E}}{r^7} - \frac{320}{3r^7} - \frac{1216\mathcal{E}}{5r^6} - \frac{128\mathcal{E}^2}{r^5}\right) + \epsilon_3\left(-\frac{126J_z^6}{r^{11}} + \frac{342J_z^4}{5r^{10}} + \frac{196J_z^4}{r^9} + \frac{7412J_z^2}{5r^8} + \frac{4344J_z^2\mathcal{E}}{5r^8} - \frac{2128J_z^2}{5r^8} + \frac{384J_z^2\mathcal{E}^2}{r^7} - \frac{376J_z^2\mathcal{E}}{r^7} + \frac{160}{3r^7} + \frac{608\mathcal{E}}{5r^6} + \frac{64\mathcal{E}^2}{r^5} + \frac{64}{3r^5} + \frac{512\mathcal{E}}{15r^4} + \frac{64\mathcal{E}^2}{5r^3}\right), \end{split}$$

$$\dot{J}_{z} = \frac{144J_{z}\mathcal{E}}{5r^{3}} + \frac{32J_{z}}{r^{4}} - \frac{24J_{z}^{3}}{r^{5}} + a\left(\frac{140J_{z}^{4}}{r^{7}} - \frac{7004J_{z}^{2}}{15r^{6}} + \frac{8\left(395 - 474J_{z}^{2}\mathcal{E}\right)}{15r^{5}} + \frac{1248\mathcal{E}}{5r^{4}} + \frac{256\mathcal{E}^{2}}{5r^{3}}\right) \\
+ \alpha_{13}\left(-\frac{216J_{z}^{3}}{r^{7}} + \frac{2016J_{z}}{5r^{6}} + \frac{336J_{z}\mathcal{E}}{r^{5}}\right) + \alpha_{52}\left(\frac{1056J_{z}^{5}}{5r^{8}} - \frac{608J_{z}^{3}}{r^{7}} + \frac{336J_{z}\mathcal{E}}{r^{5}}\right) \\
+ \frac{288\left(7J_{z} - 6J_{z}^{3}\mathcal{E}\right)}{5r^{6}}\right) + \epsilon_{3}\left(-\frac{42J_{z}^{5}}{r^{9}} - \frac{666J_{z}^{3}}{5r^{8}} + \frac{12\left(-10J_{z}^{3}\mathcal{E} + 9J_{z}^{3} + 37J_{z}\right)}{r^{7}}\right) \\
+ \frac{24\left(151J_{z}\mathcal{E} - 42J_{z}\right)}{5r^{6}} + \frac{24\left(12J_{z}\mathcal{E}^{2} - 7J_{z}\mathcal{E}\right)}{r^{5}}\right). \tag{4.7}$$

In principle, the motion of the stable orbits is restricted to a region whose shape can be determined by  $(\mathcal{E}, J_z, \mathcal{Q} + J_z^2)$ . An equivalent way to describe the motion is to specify  $(p, e, \iota)$  [98], where  $\iota$  is the inclination angle. Also we have:  $r_{p,a} = \frac{p}{1 \pm e}$  and  $\cos \iota = \frac{J_z}{(\mathcal{Q} + J_z^2)^{1/2}}$ ;  $r_{p,a}$  are the turning points. Since we are considering equatorial orbits, the motion will be characterized by  $(\mathcal{E}, J_z)$  or equivalently (p, a) as  $\iota = 0$  and  $\mathcal{Q} = 0$ . Then using radial equation Eq.(A.17), at the turning points  $(\mathcal{E}, J_z)$  become

$$\mathcal{E} = \frac{(1 - e^2)}{p} \left[ -\frac{1}{2} - \frac{a(1 - e^2)}{p^{3/2}} + \frac{\alpha_{13}(1 - e^2)}{2p^2} - \frac{\epsilon_3(1 - e^2)}{4p^2} \right],$$

$$J_z = \sqrt{p} - \frac{a(e^2 + 3)}{p} + \frac{\alpha_{13}(e^2 + 3)}{2p^{3/2}} + \frac{\alpha_{52}(1 - e^2)}{2p^{3/2}} - \frac{\epsilon_3(e^2 + 3)}{4p^{3/2}}.$$
(4.8)

These results, in linear order a, coincide with the ones presented in [91] without the deviation parameters. Here, we take leading order contributions from the deviation parameters and discard subleading terms. Also, we make use of  $E = \mu + \mathcal{E}$  as discussed in Appendix (A). Plugging Eq.(4.8) into Eq.(4.7), the instantaneous fluxes become

$$\dot{\mathcal{E}} = \frac{16e^4}{5p^2r^3} - \frac{32e^2}{5p^2r^3} + \frac{256e^2}{15pr^4} + \frac{136e^2}{5r^5} + \frac{16}{5p^2r^3} - \frac{256}{15pr^4} - \frac{88}{15r^5} + \frac{160p}{3r^6} - \frac{40p^2}{r^7}$$

$$+ a\left(-\frac{3688^{3/2}}{5r^8} + \frac{196p^{5/2}}{r^9} + \frac{2920\sqrt{p}}{3q^7} - \frac{64e^6}{5p^{7/2}r^3} + \frac{192e^4}{5p^{7/2}r^3} - \frac{192e^2}{5p^{7/2}r^3} + \frac{64}{5p^{7/2}r^3} \right)$$

$$- \frac{512e^4}{15p^{5/2}r^4} + \frac{1024e^2}{15p^{5/2}r^4} - \frac{512}{15p^{5/2}r^4} - \frac{512e^4}{5p^{3/2}r^5} - \frac{64e^2}{5p^{3/2}r^5} + \frac{576}{5p^{3/2}r^5} + \frac{64e^2}{\sqrt{p}r^6} - \frac{1472}{3\sqrt{p}r^6}$$

$$- \frac{16e^2\sqrt{p}}{r^7} + \alpha_{13} \left( \frac{32e^6}{5p^4r^3} - \frac{96e^4}{5p^4r^3} + \frac{152e^4}{15p^3r^4} + \frac{152e^4}{5p^2r^5} + \frac{96e^2}{15p^3r^3} - \frac{1024e^2}{15p^5} \right)$$

$$+ \frac{296e^2}{r^7} - \frac{32}{5p^4r^3} + \frac{256e}{15p^3r^4} - \frac{4188}{5p^2r^5} + \frac{2168}{5p^2r^5} - \frac{2168e^2}{15p^3r^4} + \frac{122e^4}{5p^2r^5} + \frac{64e^2}{15p^3r^4} - \frac{1024e^2}{5p^2r^5} \right)$$

$$+ \frac{264e^4}{p^6} + \frac{592e^2}{5p^2r^5} - \frac{454e^2}{15p^6} + \frac{10952e^2}{15p^7} - \frac{2176pe^2}{5r^8} - \frac{296e}{5p^2r^5} + \frac{3584}{15p^6} - \frac{4184}{5r^7} + \frac{7872p}{5r^8}$$

$$- \frac{20192p^2}{15p^9} + \frac{2048p^3}{5r^{10}} \right) + e_3\left( \frac{32e^8}{5p^5r^3} - \frac{15e^6}{5p^4r^3} + \frac{256e^4}{5p^4r^4} + \frac{256e^4}{5p^3r^5} + \frac{48e^4}{5p^4r^3} - \frac{128e^4}{5p^5r^5} + \frac{128e^4}{15p^4r^4} \right)$$

$$+ \frac{256e^4}{15p^4} - \frac{56e^4}{5p^2r^5} + \frac{272e^4}{p^3r^5} + \frac{460e^4}{p^3r^6} + \frac{16e^4}{p^6} - \frac{48e^2}{5p^5r^3} + \frac{256e^2}{15p^3r^3} + \frac{256e^2}{256e^2} - \frac{256e^2}{3p^3r^4} - \frac{32e^2}{5p^5r^3}$$

$$- \frac{272e^2}{15p^3r^5} + \frac{5160e^2}{3p^2r^5} + \frac{160e^4}{p^3r^5} + \frac{68e^2}{p^3r^5} + \frac{256e^2}{5p^5r^3} + \frac{256e^2}{15p^3r^4} - \frac{32e^2}{5p^5r^3} + \frac{256e^4}{15p^3r^4} + \frac{256e^4}{3p^3r^5} + \frac{256e^4}{3p^3r^5} + \frac{256e^4}{5p^3r^3} + \frac{256e^4}{5p^3r^3}$$

With the instantaneous fluxes in hand, let us now determine the average rate change of these quantities. We take the average within adiabatic approximation [78,105,106], where it is justifiable to consider the motion of the inspiralling object on a geodesic. In other words, as long as we

are concerned with timescales much shorter than the radiation reaction time scale, the adiabatic approximation is useful to consider the motion of the particle to be geodesic [97]. The radiative losses will cause  $(\dot{\mathcal{E}}, \dot{J}_z)$  to vary slowly, and  $(\langle \dot{\mathcal{E}} \rangle, \langle \dot{J}_z \rangle)$  are estimated by taking the average over one orbit. Thus, in general, the expression for average fluxes can be written as

$$\langle \dot{C} \rangle = \frac{1}{T_r} \int_0^{2\pi} \dot{C}(\chi) \frac{dt}{d\chi} d\chi \quad ; \quad C \equiv (\mathcal{E}, J_z).$$
 (4.11)

It is to be noted that higher-order PN terms (at 3PN order) proportional to  $\epsilon_3$  coefficient coming from Eq.(4.9, 4.10) after averaging are discarded (these are associated with a  $\frac{1}{p^8}$  factor in energy flux and  $\frac{1}{p^{13/2}}$  in the angular momentum flux.) as we are at this point only interested in the leading order contribution coming from the deviation parameters. As we will discuss below, the leading order contribution will appear at the 2PN order. We similarly discard this higher-order correction in orbital evolution, phase and dephase. For calculating  $T_r$ , we make use of parametrization Eq.(3.7) and radial velocity; the time period with the leading corrections reads as

$$T_r = \frac{\pi}{\sqrt{1 - e^2}} \left[ \frac{2p^{3/2}}{(1 - e^2)} - 6a + \frac{1}{\sqrt{p}} \left( 3\alpha_{13} - \alpha_{52} - \frac{3\epsilon_3}{2} \right) \right]. \tag{4.12}$$

Using Eqs.(4.9, 4.10) and Eq.(4.12), the average loss of energy and angular momentum fluxes are given by

$$\left\langle \frac{d\mathcal{E}}{dt} \right\rangle = -\frac{\left(1 - e^2\right)^{3/2}}{15p^5} \left[ \left( 37e^4 + 292e^2 + 96 \right) - \left\{ \frac{a}{p^{3/2}} \left( \frac{491e^6}{2} + 2847e^4 + 3292e^2 + 584 \right) \right. \right.$$

$$\left. - \frac{\alpha_{13}}{p^2} \left( 251e^6 + 4035e^4 + 5532e^2 + 864 \right) + \frac{\alpha_{52}}{p^2} \left( \frac{2775e^6}{4} + 2275e^4 - 130e^2 - 98e^2\sqrt{1 - e^2} \right) \right.$$

$$\left. - 48\sqrt{1 - e^2} + \frac{37e^6\sqrt{1 - e^2}}{2} + \frac{255e^4\sqrt{1 - e^2}}{2} - 240 \right) + \frac{\epsilon_3}{p^2} \left( \frac{251e^6}{2} + \frac{4035e^4}{2} + 2766e^2 + 432 \right) \right\} \right],$$

$$\left\langle \frac{dJ_z}{dt} \right\rangle = -\frac{\left(1 - e^2\right)^{3/2}}{5p^3} \left[ \frac{4}{p^{1/2}} \left( 7e^2 + 8 \right) - \frac{a}{3p^2} \left( 549e^4 + 1428e^2 + 488 \right) + \frac{2\alpha_{13}}{p^{5/2}} \left( 84e^4 + 361e^2 + 120 \right) \right.$$

$$\left. - \frac{\alpha_{52}}{2(1 - e^2)^{1/2}p^{5/2}} \left\{ \left( -28e^6 + 24e^4 + 36e^2 - 32 \right) + \sqrt{1 - e^2} \left( 12e^6 + 421e^4 + 192e^2 - 128 \right) \right\}$$

$$\left. - \frac{\epsilon_3}{p^{5/2}} \left( 84e^4 + 361e^2 + 120 \right) \right].$$

$$(4.14)$$

Expressions Eq.(4.13) and Eq.(4.14) show average energy and angular momentum fluxes in the leading order corrections of spin and deviation parameters, which match with the standard results of [70,91,97,107,108] in the equatorial limit when the deviation parameters are turned off. We know

that the leading order term coming from GR, in various fluxes, appears with a  $\mathcal{O}(c^{-5})$  factor [107]<sup>7</sup>. Then, one can easily check that, after restoring the factors of c, the leading correction due to the spin from the GR part shows up at 1.5PN order, and the correction due to the deviation parameters first appears at the 2PN order. Let us now examine the orbital evolution of the inspiralling object. Since our analysis holds within the adiabatic approximation, one can write down the following balance equations [109]

$$\left\langle \frac{d\mathcal{E}}{dt} \right\rangle_{GW} = -\left\langle \frac{d\mathcal{E}}{dt} \right\rangle \quad ; \quad \left\langle \frac{dJ_z}{dt} \right\rangle_{GW} = -\left\langle \frac{dJ_z}{dt} \right\rangle.$$
 (4.15)

This means that, in the adiabatic approximation, the averaged radiated energy and angular momentum flux are equivalent to the orbital energy and angular momentum loss. It provides the GW fluxes that match with [107,110]. We use Eq.(4.13) and Eq.(4.14) for computing the average rate change of eccentric orbital parameters, which can be obtained from the following relation

$$\frac{d\mathcal{E}}{dt} = \frac{\partial \mathcal{E}}{\partial p} \frac{dp}{dt} + \frac{\partial \mathcal{E}}{\partial e} \frac{de}{dt} \quad ; \quad \frac{dJ_z}{dt} = \frac{\partial J_z}{\partial p} \frac{dp}{dt} + \frac{\partial J_z}{\partial e} \frac{de}{dt}. \tag{4.16}$$

Here, we use the average loss of energy and angular momentum fluxes. Then we get,

$$\left\langle \frac{dp}{dt} \right\rangle = \left( \frac{\dot{\mathcal{E}} \partial_e J_z - \dot{J}_z \partial_e \mathcal{E}}{\partial_p \mathcal{E} \partial_e J_z - \partial_e \mathcal{E} \partial_p J_z} \right) \quad ; \quad \left\langle \frac{de}{dt} \right\rangle = \left( \frac{\dot{J}_z \partial_p \mathcal{E} - \dot{\mathcal{E}} \partial_p J_z}{\partial_p \mathcal{E} \partial_e J_z - \partial_e \mathcal{E} \partial_p J_z} \right). \tag{4.17}$$

Using Eq.(4.7), Eq.(4.8) and Eq.(4.12) and further taking the average of the resultant expression or directly using Eq.(4.13) and Eq.(4.14), the average rate change of (p, e) are given by

$$\left\langle \frac{dp}{dt} \right\rangle = -\frac{2(1 - e^2)^{3/2}}{5p^3} \left[ 4\left(7e^2 + 8\right) - \frac{a}{3p^{3/2}} \left(475e^4 + 1516e^2 + 1064\right) + \frac{\alpha_{13}}{3p^2} \left(1152 + 2384e^2 + 509e^4\right) \right]$$

$$+ \frac{\alpha_{52} \left(1 - e^2\right)^{3/2}}{15p^5} \left(36e^6 + 1273e^4 - 12\left(7e^2 + 8\right) \left(1 - e^2\right)^{3/2} + 4e^2 - 672\right)$$

$$+ \frac{\epsilon_3 \left(1 - e^2\right)^{3/2}}{15p^5} \left[1152 + 2384e^2 + 509e^4\right],$$

$$(4.18)$$

$$\langle \frac{d\mathcal{E}}{dt} \rangle \sim -\frac{1}{p^5 \, c^5} \big( a_1 + a_2 \frac{a}{p^{3/2} \, c^3} + a_3 \frac{\alpha_{13}}{p^2 \, c^4} + a_4 \frac{\alpha_{52}}{p^2 \, c^4} + a_5 \frac{\epsilon_3}{p^2 \, c^4} \big), \ \\ \langle \frac{dJ_z}{dt} \rangle \sim -\frac{1}{p^3 \, c^5} \big( a_6 \frac{1}{p^{1/2}} + a_7 \frac{a}{p^2 \, c^3} + a_8 \frac{\alpha_{13}}{p^{5/2} \, c^4} + a_9 \frac{\alpha_{52}}{p^{5/2} \, c^4} + a_{10} \frac{\epsilon_3}{p^{5/2} \, c^4} \big).$$

After pulling out an overall factor of  $\frac{1}{c^5}$  we can identify the PN order n,  $(\frac{v}{c})^{2n}$  at which the deviation parameters contribute to the fluxes. $a_i$ ,  $i=1,\cdots 10$  are just some eccentricity (e) dependant constant pre-factors.

<sup>&</sup>lt;sup>7</sup>Restoring the factors of c, we can see that the expressions for the fluxes take the following form:

$$\left\langle \frac{de}{dt} \right\rangle = -\frac{e\left(1 - e^2\right)^{3/2}}{15p^4} \left[ 121e^2 + 304 - \frac{a}{2p^{3/2}} \left( 1313e^4 + 5592e^2 + 7032 \right) + \frac{2\alpha_{13}}{p^2} \left( 385e^4 + 2664e^2 + 2292 \right) \right] 
+ \frac{\alpha_{52} \left(1 - e^2\right)^{3/2}}{60ep^6} \left( 72e^8 + 5249e^6 + 6562e^4 - 2e^2 \left( 121e^2 + 304 \right) \left( 1 - e^2 \right)^{3/2} - 1872e^2 + 384 \right) 
+ \frac{\epsilon_{3}e \left( 1 - e^2 \right)^{3/2}}{60p^6} \left[ 9168 + 10656e^2 + 1540e^4 \right].$$
(4.19)

The semi-latus rectum (p) and the eccentricity (e) decrease with time, as long as the contributions coming from the terms proportional to the deformation parameters are subleading, as a result of gravitational radiation since the sign of the leading terms in right sides of Eq.(4.18) and Eq.(4.19) are negative. Here, one can also easily track the leading PN orders for various correction terms due to the spin and the deformation parameters similar to the flux expressions. Again, we can see by restoring powers of c, the contribution of leading order corrections coming from the deviation parameters emerge at 2PN order.

One can further examine how long it takes for the inspiralling object to reach the LSO. It will depend on the relative signs of the deviation parameters and their corresponding LSO values from Eq.(3.6). We use Eq.(4.18) and integrate it from the starting point of the inspiral p = 14 to  $p = p_{sp}$  for determining the time it takes to reach LSO. More precisely, we will consider that change of this time scale, denoted by  $\Delta t$ , due to the presence of the deviation parameters compared to that of GR. Hence, after integrating Eq.(4.18) to find the time scale, we subtract the GR part from it. Finally, we get

$$\Delta t \approx \frac{(1 - e^2)^{-3/2}}{(8 + 7e^2)^2} \left[ -\frac{5}{192} (1152 + 2384e^2 + 509e^4)(196 - p_{sp}^2)(\alpha_{13} - \frac{\epsilon_3}{2}) + \frac{5\alpha_{52}}{384} \left( 36e^6 - 96(7 + \sqrt{1 - e^2}) + 4e^2(1 + 3\sqrt{1 - e^2}) + e^4(1273 + 84\sqrt{1 - e^2}) \right) (196 - p_{sp}^2) \right].$$

$$(4.20)$$

where one should only consider the GR part in the expression for  $p_{sp}$  defined in Eq.(3.6) as we are working only in linear order of the deviation parameters. Note that the PN corrections coming from the GR part will be cancelled in  $\Delta t$ . This then estimates the change of time required by the test body to reach LSO due to the deviation parameters only. Thus, these features imply the measurable effects of the Johannsen parameters. Also it is evident from Eq.(4.20), this change of the time scale for the secondary to reach LSO, depends on the relative magnitude of the deviation parameters. Depending on that, if  $\Delta t$  becomes negative, then it corresponds to the fact that the secondary takes less time to reach LSO when the deviation parameters are turned on. Next, to analyze the detectability of deviations in the Kerr black hole, we next examine the orbital phase and GW dephasing.

<sup>&</sup>lt;sup>8</sup>The relative changes in (p(t), e(t)) after subtracting out the GR contribution as a function of time have been presented in the Appendix (B) for distinct values of deviation parameters.

# 5 Detection prospects with GW dephasing

This section examines the prospects of detecting deviations from the Kerr black hole by considering an EMRI system. As mentioned earlier in Sec. (3), the eccentric motion exhibits two fundamental frequencies  $(\Omega_{\phi}, \Omega_r)$ , that is, angular and radial, respectively. In principle, both frequencies have contributions in the phase computation and collectively can be written as

$$\frac{d\varphi_i}{dt} = \langle \Omega_i(p(t), e(t)) \rangle = \frac{1}{T_r} \int_0^{2\pi} d\chi \frac{dt}{d\chi} \Omega_i(p(t), e(t), \chi) \quad ; \quad i = (\phi, r), \tag{5.1}$$

where (p(t), e(t)) will be obtained from Eq.(4.18) and Eq.(4.19).  $\langle \Omega_i(p(t), e(t)) \rangle$  denotes the orbital averaged frequency. We primarily focus on the azimuthal phase shift regulating the orbital dephasing:  $\varphi_{\phi}(t) \sim \phi(t)$  [89,111]. We take the initial phase to be zero ( $\varphi_i(0) = 0$ ). With this, using Eq.(A.17), the corresponding expression is given by

$$\frac{d\phi}{dt} = \frac{\left(1 - e^2\right)^{3/2}}{p^{3/2}} - \frac{a\left(1 - e^2\right)^{3/2}}{p^3} \left(3e^2 + 1\right) + \frac{\alpha_{52}\left(1 - e^2\right)}{4p^{7/2}} \left(2e^4 - \left(3\sqrt{1 - e^2} + 4\right)e^2 + 2\right) + \frac{3(1 - e^2)^{3/2}(1 + e^2)}{2p^{7/2}} \left(\alpha_{13} - \frac{\epsilon_3}{2}\right).$$
(5.2)

Note that here (p,e) are functions of time and are obtained from Eq.(4.18) and Eq.(4.19) that help us further in solving the Eq.(5.2) to find  $\phi(t)$ . We use the Mathematica-based built-in function NDSolve to determine the time evolution of the orbital parameters and phase. Also note that, structure of phase  $\phi(t)$  is the following:  $\phi(t) \sim \frac{1}{c^0} - \frac{a}{c^3} + \frac{\alpha_{52}}{c^4} + \frac{\alpha_{13}}{c^4} - \frac{\epsilon_3}{c^4}$ . The deviation parameters enter at 2PN order. At this point, note that the complete expression for the phase up to 2PN order will require the addition of the GR contributions at 1PN-2PN order, including the correction due to the spin parameter. However, we will eventually focus on the dephasing, subtracting the GR contribution. Hence, we will not consider these higher-order PN terms for GR. Interested readers are referred to [112] for more details.

Let us now analyze the effects of deviation parameters in GW dephasing that will implicate the possible detectability of deformations in Kerr black holes. We use the fact that the GW dephasing is twice the orbital phase, i.e.,  $\Phi_{\rm GW}=2\phi(t)$ . We use an EMRI system with a Johannsen black hole as the reference waveform to study the GW signals for possible deviations from the Kerr black hole. The dephasing between a Johannsen spacetime and a Kerr black hole, up to a given time  $t_{\rm obs}$ , is defined as

$$\Delta\Phi(t_{\rm obs}) = |\Phi_{\rm GW}^{\rm JHN}(t_{\rm obs}) - \Phi_{\rm GW}^{\rm Kerr}(t_{\rm obs})|, \tag{5.3}$$

where  $\Phi_{\rm GW}^{\rm JHN}$  represents the GW phase from the Johannsen spacetime and  $\Phi_{\rm GW}^{\rm Kerr}$  represents the GW phase from the Kerr black hole. Their difference provides us with the GW dephasing. We analyze

our results taking the observation period one year ( $t_{\rm obs} = 1$  year). As we are considering an EMRI system, we take the primary black hole with the mass  $M = 10^6 M_{\odot}$  and the secondary with the mass  $\mu = 10 M_{\odot}$ . This sets up the mass ratio  $q = 10^{-5}$ . We consider  $p_{\rm in} = 14$  to be the start of the inspiral with distinct initial eccentricities ( $e_{\rm in}$ ).

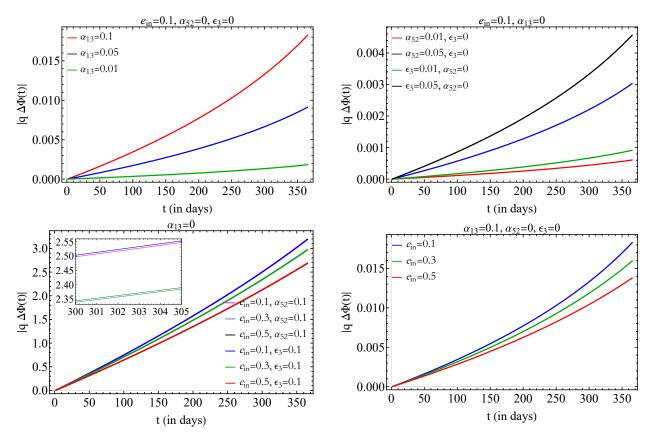


Figure 1: The plots represent the dephasing  $\Delta\Phi$  in one year of observation time. We consider an EMRI system with the mass of the primary black hole  $M=10^6M_{\odot}$  and the secondary with the mass  $\mu=10M_{\odot}$ , setting up the mass ratio  $q=10^{-5}$ . The upper panel shows the dephasing for different values of  $(\alpha_{13}, \alpha_{52}, \epsilon_3)$  with  $e_{\rm in}=0.1$ . The lower panel shows the same for different initial eccentricities.

In Fig.(1)<sup>9</sup> we show the effects of Johannsen parameters on GW dephasing for different initial eccentricities ( $e_{\rm in}$ ). Notably, the dephasing eventually depends on the relative signs of the deviation parameters as expressed in Eq. (5.2). The upper panel shows that (for  $e_{\rm in} = 0.1$ ), the larger the strength of the deviation parameter, the larger the dephasing is. In the lower panel, interestingly, the small eccentricities give rise to a relatively higher magnitude of the dephasing than others.

<sup>&</sup>lt;sup>9</sup>One can set  $e_{\rm in}=0$  in Eqs. (4.18, 5.2), and obtain the dephasing analytically in the frequency domain:  $\Delta\Phi=\frac{25}{16q(M\Omega)^{1/3}}(\alpha_{13}+\alpha_{52}-\epsilon_3/2)$ . Then, we can provide an order of magnitude estimate of it in the following way. Given the reference [113], we consider  $M\sim 140M_{\odot}$ ,  $q\sim 0.60$ . And then setting  $\alpha_{13}=0.1$  (and other parameters to be zero) along with the allowed frequency range mentioned in Table (V) of [113], the  $\Delta\Phi$  comes out to be in the range of  $10^{-2}-10^{-3}$  which is consistent with the deviation at 2 PN order ( $\delta\varphi_4$ ) ~ 0.26 as shown in Table (VI) of [113]. Using a similar analysis, we can also show that even when  $\alpha_{52}$  and  $\epsilon_3\sim 0.1$ , the dephasing is consistent with what comes from LIGO data [113].

Hence, the dynamics of the inspiralling object, even with lower eccentricity, make the detectability of deviations from the Kerr black hole more promising with LISA. Furthermore, since the secondary object will encounter a strong gravitational field in the vicinity of the last stable orbit, the higher-order PN corrections or the black hole perturbation approach are needed to compute the GW phase more accurately, which will help us more concretely understand this behaviour at late time. Moreover, with an average signal-to-noise ratio (SNR) of about 30 for LISA observations, it should be able to detect the dephasing with  $\Delta\Phi \gtrsim 0.1$  rad [114]. Note that Johannsen parameters, bringing deviations from the Kerr black hole, cause the dephasing to be proportional to  $\mathcal{O}(1/q)$ , implying the dependence on the mass ratio and, as a result, giving rise to the notion of detectability from LISA observations.

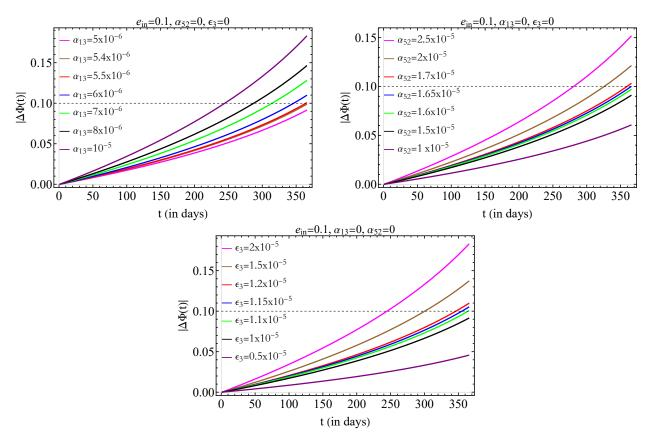


Figure 2: The plots provide an order of magnitude estimate of the upper bound on the deviation parameters when  $|\Delta\Phi| < 0.1$ . We set mass ration  $q = 10^{-5}$  and  $e_{\rm in} = 0.1$ .

Last but not least, we examine the order of magnitude of the upper bound that these Johannsen parameters will have in case LISA cannot detect dephasing associated with these deviation parameters, i.e. when  $|\Delta\Phi| < 0.1$ . This is shown in Fig. (2). We consider  $q = 10^{-5}$  and  $e_{\rm in} = 0.1$ , and for  $\alpha_{13} \lesssim 5.5 \times 10^{-6}$ ,  $\alpha_{52} \lesssim 10^{-5}$  and  $\epsilon_3 \lesssim 10^{-5}$ , the dephasing  $|\Delta\Phi(t)|$  remains less than 0.1 till the end of the evolution as can be seen from Fig. (2). This gives an order of magnitude estimate

of the upper bound for deviation parameters in case we cannot detect the dephasing using LISA.

## 6 Discussion

One of the key research objectives of the LISA mission is to map Kerr spacetime [115]. To conduct such a major test of GR, we need to be able to set up the required tools that can measure any deviations from the Kerr metric. This will offer deep insights into the weak and strong gravity regimes of the supermassive black hole (SMBH) that can capture a stellar-mass object which emits gravitational radiation while inspiralling the SMBH. The generated GWs carry information of the spacetime geometry, hence acting as a probe for the GR test. In this direction, EMRIs are the perfect astrophysical objects for testing GR with LISA; thus, the comprehensive mapping of the spacetime metric, where the inspiralling object moves, should be made possible by the detection of GWs from EMRIs [116]. Here, we attempt to analyze such a notion, which brings the deviations in Kerr metric and can have possible detectability through low-frequency detectors.

We consider the Johannsen spacetime that carries four parameters  $(\alpha_{13}, \alpha_{52}, \epsilon_3, \alpha_{22})$  which infer the deviations from the Kerr black hole [93, 117]. The broader scope of deviations is somewhat restricted by the perturbative method. We limit the deformation parameters in the metric to small deviations from the GR solution. Hence, we examine our results with leading order PN corrections. We determine the eccentric equatorial orbital motion of the inspiralling object and find the expression for the last stable orbit, i.e., the truncation region of the inspiralling object, which complies with [97]. We perform our analysis within the adiabatic approximation that breaks down beyond the LSO; therefore, we confine the motion in the domain  $(p_{\rm in} = 14, p_{\rm min}(e))$ . We analytically calculate instantaneous fluxes and compute GW fluxes. With the average loss of energy and angular momentum fluxes, we obtain the expressions for orbital evolution parameters (p(t), e(t)) and estimate how long it takes for the inspiralling object to reach the LSO. We also analyse the relative change in eccentric orbital parameters due to the effect of deformations and find that the relative change in (p(t), e(t)) increases with a larger magnitude of deviations. Note that all results with the Kerr limit in slow-rotation approximation are in agreement with [91] if considered non-equatorial orbits.

Next, we estimate GW dephasing and further analyze the detection prospects of deviations from the Kerr black hole with the mass ratio  $q = 10^{-5}$ . We find that the changes in deviation parameters, shown in Fig. (1), cause dephasing to be prominent from the detection perspective as it goes as  $\mathcal{O}(1/q)$ . We observe that the leading order corrections from the deviation parameters appear at 2PN, whereas spin contributes at 1.5PN. We have ignored the general relativistic 1PN-2PN contributions <sup>10</sup> in the calculations as our main goal was to study the dephasing. The PN terms of GR contributing to final results would be eliminated as we are computing the phase difference

<sup>&</sup>lt;sup>10</sup>However, readers are suggested to refer [112] for comprehensive details of GR contributions up to 3PN order.

between the Johannsen and Kerr case. It turns out that  $\alpha_{22}$  does not play any role to the results derived in the leading order PN corrections; however, other parameters  $(a, \alpha_{13}, \alpha_{52}, \epsilon_3)$  provide measurable effects. We further notice that  $\epsilon_3$  generates a relatively larger dephasing than the other parameters present in the metric. The larger the deviation parameters are, the more dephasing there is. Further, the dynamics with lower initial eccentricities produce larger dephasing. Since we know that observations over the year with the average SNR 30, LISA should detect dephasing  $\Delta \Phi \gtrsim 0.1$  rad [114]; thus, our analysis provides measurable effects with such low-frequency detectors. We have also provided an estimate for the upper bound of these deviation parameters in case LISA can not detect the associated dephasing.

However, we strongly expect that the higher-order PN corrections will be an interesting addition to such an analysis, which we hope to communicate in our upcoming studies. Another direction to explore these scenarios is the black hole perturbation [118,119] that can more concretely improvise the PN results and can constrain the deviation parameters with their possible detectability. If LISA might impose interesting limits on non-GR deviations/deformations, it is an intriguing topic that could be addressed with the aid of the Johannsen framework. In order to execute such an analysis, one needs to evolve geodesics in this background and develop the corresponding GWs. To quantify more precisely the magnitude of the non-GR deviations from the Kerr black hole using LISA observations, one might next perform a Fisher type of analysis [120]. These are some of the aspects that will advance the understanding of deviations in Kerr, which we would like to explore in future studies.

# Acknowledgements

S. K. would like to thank Mostafizur Rahman for useful discussions. A.B. would like to thank the speakers of the workshop "Testing Aspects of General Relativity-II" (11-13th April 2023) and "New insights into particle physics from quantum information and gravitational waves" (12-13th June 2023) at Lethbridge University, Canada, funded by McDonald Research Partnership-Building Workshop grant by McDonald Institute for useful discussions. Research of S. K. is supported by the research grant (202011BRE03RP06633-BRNS) by the Board of Research In Nuclear Sciences (BRNS), Department of Atomic Energy (DAE), India. A. C. is supported by the Prime Minister's Research Fellowship (PMRF-192002-1174) of the Government of India. A.B. is supported by the Mathematical Research Impact Centric Support Grant (MTR/2021/000490) by the Department of Science and Technology Science and Engineering Research Board (India) and the Relevant Research Project grant (202011BRE03RP06633-BRNS) by the Board Of Research In Nuclear Sciences (BRNS), Department of Atomic Energy (DAE), India. A.B. also acknowledge associateship program of Indian Academy of Science, Bengaluru. Authors would like to thank the anonymous referee for useful comments and suggestions.

## A Geodesic velocities and constants of motion

In this section, we derive velocity components of geodesic motion exhibited by the inspiralling object in the Johannsen background. Here, we obtain the equations without setting the equatorial assumption. We implement the Hamilton-Jacobi formalism; the action for which is given as [92,93]

$$S = \frac{1}{2}\mu^2\tau - Et + J_z\phi + R(r) + \Theta(\theta), \tag{A.1}$$

and we have

$$-\frac{\partial S}{\partial \tau} = \frac{1}{2} g^{\alpha\beta} \frac{\partial S}{\partial x^{\alpha}} \frac{\partial S}{\partial x^{\beta}}.$$
 (A.2)

with  $p_{\alpha} = \partial S/\partial x^{\alpha}$  and  $\partial S/\partial \tau = \mu^2/2$ . The separable equations in radial and angular terms take the following form

$$\Delta A_5 \left(\frac{dR}{dr}\right)^2 - \frac{1}{\Delta} \left(A_1(r^2 + a^2)E - aA_2J_z\right)^2 + \mu^2 \left(r^2 + \epsilon_3 \frac{M^3}{r}\right) = -Q,\tag{A.3}$$

$$\left(\frac{d\Theta}{d\theta}\right)^2 + a^2\mu^2\cos^2\theta + \left(aE\sin\theta - \frac{J_z}{\sin\theta}\right)^2 = Q. \tag{A.4}$$

Carter constant is given as:  $Q \equiv Q - (J_z - aE)^2$ . The functions R(r) and  $\Theta(\theta)$  can further be related to the respective momenta of the particle,

$$\frac{dR}{dr} = \frac{\mu \Sigma}{\Delta A_5} \frac{dr}{d\tau} \qquad ; \qquad \frac{d\Theta}{d\theta} = \mu \Sigma \frac{d\theta}{d\tau} \,. \tag{A.5}$$

Thus, the Eq.(A.3) and Eq.(A.4) can be written as

$$\mu^{2} \left(\frac{dr}{d\tau}\right)^{2} = \frac{A_{5}}{\Sigma^{2}} \left[ \left( A_{1}(r^{2} + a^{2})E - aA_{2}J_{z} \right)^{2} - \Delta \left( Q + \mu^{2}r^{2} + \mu^{2}\epsilon \frac{M^{3}}{r} \right) \right], \tag{A.6}$$

$$\mu^2 \left(\frac{d\theta}{d\tau}\right)^2 = \frac{1}{\Sigma^2} \left[ (Q - a^2 \mu^2 \cos^2 \theta) - \left( aE \sin \theta - \frac{J_z}{\sin \theta} \right)^2 \right]. \tag{A.7}$$

Since we have two conserved quantities- energy and angular momentum, we can obtain the following relations,

$$\mu \frac{dt}{d\tau} = \frac{1}{\mathcal{C}} \left[ N \left( A_1 \left( a^2 + r^2 \right) \left( a^2 A_1 E - a A_2 J_z + A_1 E r^2 \right) - a^2 \Delta E \sin^2(\theta) + a \Delta J_z \right) \right], \tag{A.8}$$

$$\mu \frac{d\phi}{d\tau} = \frac{1}{\mathcal{C}} \left[ N \left( aA_2 \left( a^2 A_1 E - aA_2 J_z + A_1 E r^2 \right) - a\Delta E + \Delta J_z \csc^2 \theta \right) \right], \tag{A.9}$$

where  $C = \Delta \Sigma \left( A_1 \left( a^2 + r^2 \right) - a^2 A_2 \sin^2(\theta) \right)^2$ . The expressions in the slow-rotation approximation become,

$$\mu \frac{dt}{d\tau} = \left[ -(r^2 A_1 A_2 - \Delta) \frac{a J_z}{r^2 \Delta} + \frac{E r^2}{\Delta} A_1^2 \right] \left( 1 + \epsilon_3 \frac{M^3}{r^3} \right)^{-1} + \mathcal{O}(a^2) , \qquad (A.10)$$

$$\mu \frac{d\phi}{d\tau} = \left[ \frac{J_z}{r^2 \sin^2 \theta} + \frac{aE}{r^2 \Delta} (A_1 A_2 r^2 - \Delta) \right] \left( 1 + \epsilon_3 \frac{M^3}{r^3} \right)^{-1} + \mathcal{O}(a^2) , \tag{A.11}$$

$$\mu^{2} \left(\frac{dr}{d\tau}\right)^{2} = \frac{A_{5}}{\Sigma^{2}} \left[ (A_{1}r^{2}E - aA_{2}J_{z})^{2} - \Delta\left(Q + \mu^{2}r^{2} + \mu^{2}\epsilon_{3}\frac{M^{3}}{r}\right) \right] + \mathcal{O}(a^{2}), \tag{A.12}$$

$$\mu^2 \left(\frac{d\theta}{d\tau}\right)^2 = \frac{1}{\Sigma^2} \left[ Q - \left( aE \sin\theta - \frac{J_z}{\sin\theta} \right)^2 \right] + \mathcal{O}(a^2). \tag{A.13}$$

In the linear-order approximation of a,  $\Sigma = r^2 + \epsilon_3 \frac{M^3}{r}$  and  $\Delta = r^2 - 2Mr$ . Using the four velocities,

$$\mu^{2} \left[ \left( \frac{dr}{d\tau} \right)^{2} + r^{2} \left( \frac{d\theta}{d\tau} \right)^{2} + r^{2} \sin^{2}\theta \left( \frac{d\phi}{d\tau} \right)^{2} \right] = (E^{2} - \mu^{2}) \left( 1 + \frac{\alpha_{52}M^{2}}{r^{2}} \right) - \frac{M^{2}(2\mu^{2}M^{2}\epsilon_{3} + \alpha_{52}Q)}{r^{4}} + \frac{2\mu^{2}M}{r} + \frac{M^{3} \left( 2\alpha_{13}E^{2} + \epsilon_{3} \left( \mu^{2} - 2E^{2} \right) + 2\alpha_{52}\mu^{2} \right) + 2MQ}{r^{3}}$$

$$+ \frac{M^{3} \left( 2\alpha_{13}E^{2} + \epsilon_{3} \left( \mu^{2} - 2E^{2} \right) + 2\alpha_{52}\mu^{2} \right) + 2MQ}{r^{3}}$$
(A.14)

Here, we have ignored terms with  $\mathcal{O}\left(\frac{aM^2}{r^4}\right)$  and  $\mathcal{O}\left(\frac{aM}{r^3}\right)$ . Further, omitting  $\mathcal{O}(r^{-3})$ , the above expression with respect to coordinate time can be written in the following form

$$\mu^{2} \left[ \left( \frac{dr}{dt} \right)^{2} + r^{2} \left( \frac{d\theta}{dt} \right)^{2} + r^{2} \sin^{2}\theta \left( \frac{d\phi}{dt} \right)^{2} \right] = \frac{\mu^{2}}{E^{2}} \left[ E^{2} - \mu^{2} + \frac{2M}{r} (3\mu^{2} - 2E^{2}) + \frac{M^{2}}{r^{2}} \left( E^{2} (4 + \alpha_{52}) - (12 + \alpha_{52})\mu^{2} \right) \right]. \tag{A.15}$$

Replacing  $E = \mu + \mathcal{E}$  [70,121,122] for separating out the rest mass energy and considering terms linear order in  $\mathcal{E}$  and ignoring  $\mathcal{O}(\mathcal{E}M/r)$  with their higher order terms. Following [123], we define

$$\mathcal{E} = \frac{\mu}{2} \left[ \left( \frac{dr}{dt} \right)^2 + r^2 \left( \frac{d\theta}{dt} \right)^2 + r^2 \sin^2 \theta \left( \frac{d\phi}{dt} \right)^2 \right] - \frac{\mu M}{r} \,. \tag{A.16}$$

With this, the equatorial plane reduces the velocities in the following form<sup>11</sup>

$$\left(\frac{dr}{d\tau}\right)^{2} = 2\mathcal{E} + \frac{2}{r} - \frac{J_{z}^{2}}{r^{2}} - \frac{4aJ_{z}}{r^{3}} + \frac{2\alpha_{13}}{r^{3}} - \frac{\epsilon_{3}}{r^{3}} \left(1 - \frac{2J_{z}^{2}}{r^{2}}\right) + \frac{\alpha_{52}}{r^{3}} \left(2 - \frac{J_{z}^{2}}{r}\right),$$

$$\frac{d\phi}{d\tau} = \frac{J_{z}}{r^{2}} + \frac{2a}{r^{3}} - \frac{\epsilon_{3}J_{z}}{r^{5}}.$$
(A.17)

These velocities will be useful while computing the fluxes in the main text. However, for higher order corrections and more precise results, one should numerically integrate geodesic equations.

<sup>&</sup>lt;sup>11</sup>Since we are focusing only on leading order PN corrections in deviation parameters that arise at 2PN; as a result, we can discard term  $\frac{2J_z^2}{r^2}$  appearing with  $\epsilon_3$ .

Further, we use Eqs.(A.11, A.13) and compute,

$$\mu^2 r^4 \left[ \left( \frac{d\theta}{d\tau} \right)^2 + \sin^2 \theta \left( \frac{d\phi}{d\tau} \right)^2 \right] = Q + 2aEJ_z \left( 1 + \frac{2M}{r} + \frac{M^2 \alpha_{22}}{r^2} \right). \tag{A.18}$$

We notice that the right-hand side is linear in a and Q. We can re-write the above expression coordinate time t,

$$\mu^{2} r^{4} \left[ \left( \frac{d\theta}{dt} \right)^{2} + \sin^{2}\theta \left( \frac{d\phi}{dt} \right)^{2} \right] = Q + 2aEJ_{z} + \frac{4aEJ_{z}M}{r} + \frac{2aEJ_{z}M^{2}\alpha_{22}}{r^{2}}. \tag{A.19}$$

By introducing Q and defining,  $Q + J_z^2 \equiv Q + 2aEJ_z$ , we may further express the conserved quantity angular momentum,

$$J_z = \mu r^2 \sin^2 \theta \left( 1 + \epsilon_3 \frac{M^3}{r^3} \right) \frac{d\phi}{d\tau} - \frac{2aEM \sin^2 \theta}{r} \,. \tag{A.20}$$

The constants of motion are consistent with [70, 122]. Eq.(A.19) to  $\mathcal{O}(a)$  takes the following form,

$$\mu^2 r^4 \left[ \left( \frac{d\theta}{dt} \right)^2 + \sin^2 \theta \left( \frac{d\phi}{dt} \right)^2 \right] = \mathcal{Q} + J_z^2 + a \left( \frac{4EM}{r} + \frac{2EM^2 \alpha_{22}}{r^2} \right) \left( 1 + \epsilon_3 \frac{M^3}{r^3} \right) \mu r^2 \sin^2 \theta \frac{d\phi}{d\tau}, \quad (A.21)$$

or in the linear order corrections

$$Q + J_z^2 = \mu^2 r^4 (\dot{\theta}^2 + \sin^2 \theta \dot{\phi}^2) - 4a\mu^2 M r \dot{\phi} \sin^2 \theta.$$
 (A.22)

Since our analysis takes the equatorial consideration, the involvement of the Carter constant is not required. These constants of motion help in estimating the fluxes, and we consider mentioning them in the main text as well.

#### B Orbital evolution

Here, we analyze the relative change in eccentric orbital parameters (p(t), e(t)) over time, sourced by the deviation parameter. We define the following:

$$\Delta p(t) = \left| p^{\text{JHN}}(t) - p^{\text{Kerr}}(t) \right|, \quad \Delta e(t) = \left| e^{\text{JHN}}(t) - e^{\text{Kerr}}(t) \right|.$$

This is obtained by subtracting the PN contributions of the GR part from Eqs. (4.18, 4.19). These reflect how the orbital dynamics change due to deviation parameters alone (which enter at 2PN order as discussed in the main text) as a function of time.

Fig. (3) and Fig. (4) provide an estimate for the relative changes  $(\Delta p(t), \Delta e(t))$ . It is evident

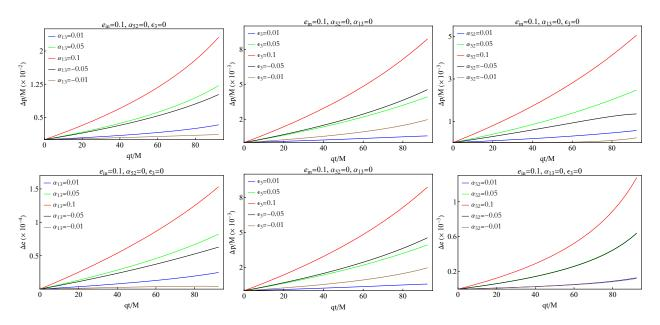


**Figure 3:** The upper panel shows the time evolution of relative change in p caused by distinct values of deviation parameters with  $e_{\rm in}$ =0.1. The lower panel provides the time evolution of relative change in orbital eccentricity with a given  $e_{\rm in}$ =0.1.

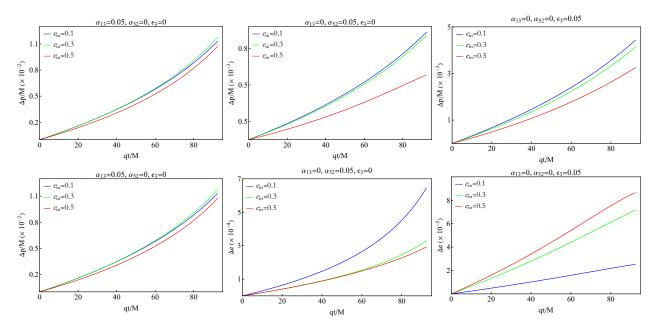


**Figure 4:** The time evolution of relative change is p (upper panel), and e (lower panel) is shown for deviation parameters  $(\alpha_{13}, \epsilon_3, \alpha_{52})$  with distinct initial eccentricities.

from the plots that these changes exhibit increasing behaviour over time; however, the order of magnitude depends on values of deviation parameters, which we have depicted in the figures.

### References

- [1] LIGO SCIENTIFIC, VIRGO collaboration, Observation of Gravitational Waves from a Binary Black Hole Merger, Phys. Rev. Lett. 116 (2016) 061102 [1602.03837].
- [2] LIGO SCIENTIFIC, VIRGO collaboration, Properties of the Binary Black Hole Merger GW150914, Phys. Rev. Lett. 116 (2016) 241102 [1602.03840].
- [3] LIGO SCIENTIFIC, VIRGO collaboration, GW151226: Observation of Gravitational Waves from a 22-Solar-Mass Binary Black Hole Coalescence, Phys. Rev. Lett. 116 (2016) 241103 [1606.04855].
- [4] LIGO SCIENTIFIC, VIRGO collaboration, GW170104: Observation of a 50-Solar-Mass Binary Black Hole Coalescence at Redshift 0.2, Phys. Rev. Lett. 118 (2017) 221101 [1706.01812].
- [5] LIGO SCIENTIFIC, VIRGO collaboration, GWTC-1: A Gravitational-Wave Transient Catalog of Compact Binary Mergers Observed by LIGO and Virgo during the First and Second Observing Runs, Phys. Rev. X 9 (2019) 031040 [1811.12907].
- [6] LIGO SCIENTIFIC, VIRGO collaboration, GWTC-2: Compact Binary Coalescences
  Observed by LIGO and Virgo During the First Half of the Third Observing Run, Phys. Rev.
  X 11 (2021) 021053 [2010.14527].
- [7] LIGO SCIENTIFIC, VIRGO, KAGRA collaboration, GWTC-3: Compact Binary Coalescences Observed by LIGO and Virgo During the Second Part of the Third Observing Run, 2111.03606.
- [8] A. Buonanno and T. Damour, Effective one-body approach to general relativistic two-body dynamics, Phys. Rev. D 59 (1999) 084006 [gr-qc/9811091].
- [9] A. Buonanno and T. Damour, Transition from inspiral to plunge in binary black hole coalescences, Phys. Rev. D 62 (2000) 064015 [gr-qc/0001013].
- [10] F. Pretorius, Evolution of binary black hole spacetimes, Phys. Rev. Lett. **95** (2005) 121101 [gr-qc/0507014].
- [11] M. Campanelli, C. O. Lousto, P. Marronetti and Y. Zlochower, Accurate evolutions of orbiting black-hole binaries without excision, Phys. Rev. Lett. 96 (2006) 111101 [gr-qc/0511048].
- [12] J. G. Baker, J. Centrella, D.-I. Choi, M. Koppitz and J. van Meter, Gravitational wave extraction from an inspiraling configuration of merging black holes, Phys. Rev. Lett. 96 (2006) 111102 [gr-qc/0511103].

- [13] Y. Mino, M. Sasaki and T. Tanaka, Gravitational radiation reaction to a particle motion, Phys. Rev. D 55 (1997) 3457 [gr-qc/9606018].
- [14] T. C. Quinn and R. M. Wald, An Axiomatic approach to electromagnetic and gravitational radiation reaction of particles in curved space-time, Phys. Rev. D 56 (1997) 3381 [gr-qc/9610053].
- [15] A. Einstein, L. Infeld and B. Hoffmann, The gravitational equations and the problem of motion, Annals of Mathematics 39 (1938) 65.
- [16] L. Blanchet, Gravitational Radiation from Post-Newtonian Sources and Inspiralling Compact Binaries, Living Rev. Rel. 17 (2014) 2 [1310.1528].
- [17] T. Damour, Gravitational scattering, post-Minkowskian approximation and Effective One-Body theory, Phys. Rev. D 94 (2016) 104015 [1609.00354].
- [18] T. Damour, High-energy gravitational scattering and the general relativistic two-body problem, Phys. Rev. D 97 (2018) 044038 [1710.10599].
- [19] R. A. Porto, The effective field theorist's approach to gravitational dynamics, Phys. Rept. 633 (2016) 1 [1601.04914].
- [20] G. Schäfer and P. Jaranowski, Hamiltonian formulation of general relativity and post-Newtonian dynamics of compact binaries, Living Rev. Rel. 21 (2018) 7 [1805.07240].
- [21] L. Barack and A. Pound, Self-force and radiation reaction in general relativity, Rept. Prog. Phys. 82 (2019) 016904 [1805.10385].
- [22] L. Barack et al., Black holes, gravitational waves and fundamental physics: a roadmap, Class. Quant. Grav. 36 (2019) 143001 [1806.05195].
- [23] M. Levi, Effective Field Theories of Post-Newtonian Gravity: A comprehensive review, Rept. Prog. Phys. 83 (2020) 075901 [1807.01699].
- [24] T. Ohta, H. Okamura, T. Kimura and K. Hiida, Physically acceptable solution of einstein's equation for many-body system, Prog. Theor. Phys. **50** (1973) 492.
- [25] P. Jaranowski and G. Schaefer, Third postNewtonian higher order ADM Hamilton dynamics for two-body point mass systems, Phys. Rev. D 57 (1998) 7274 [gr-qc/9712075].
- [26] T. Damour, P. Jaranowski and G. Schaefer, Dynamical invariants for general relativistic two-body systems at the third postNewtonian approximation, Phys. Rev. D 62 (2000) 044024 [gr-qc/9912092].

- [27] L. Blanchet and G. Faye, Equations of motion of point particle binaries at the third postNewtonian order, Phys. Lett. A 271 (2000) 58 [gr-qc/0004009].
- [28] T. Damour, P. Jaranowski and G. Schaefer, Dimensional regularization of the gravitational interaction of point masses, Phys. Lett. B 513 (2001) 147 [gr-qc/0105038].
- [29] T. Damour, P. Jaranowski and G. Schäfer, Nonlocal-in-time action for the fourth post-Newtonian conservative dynamics of two-body systems, Phys. Rev. D 89 (2014) 064058 [1401.4548].
- [30] P. Jaranowski and G. Schäfer, Derivation of local-in-time fourth post-Newtonian ADM Hamiltonian for spinless compact binaries, Phys. Rev. D 92 (2015) 124043 [1508.01016].
- [31] L. Bernard, L. Blanchet, A. Bohé, G. Faye and S. Marsat, Fokker action of nonspinning compact binaries at the fourth post-Newtonian approximation, Phys. Rev. D 93 (2016) 084037 [1512.02876].
- [32] T. Marchand, L. Bernard, L. Blanchet and G. Faye, Ambiguity-Free Completion of the Equations of Motion of Compact Binary Systems at the Fourth Post-Newtonian Order, Phys. Rev. D 97 (2018) 044023 [1707.09289].
- [33] S. Foffa and R. Sturani, Dynamics of the gravitational two-body problem at fourth post-Newtonian order and at quadratic order in the Newton constant, Phys. Rev. D 87 (2013) 064011 [1206.7087].
- [34] S. Foffa, P. Mastrolia, R. Sturani and C. Sturm, Effective field theory approach to the gravitational two-body dynamics, at fourth post-Newtonian order and quintic in the Newton constant, Phys. Rev. D 95 (2017) 104009 [1612.00482].
- [35] S. Foffa and R. Sturani, Conservative dynamics of binary systems to fourth Post-Newtonian order in the EFT approach I: Regularized Lagrangian, Phys. Rev. D 100 (2019) 024047 [1903.05113].
- [36] R. A. Porto and I. Z. Rothstein, Apparent ambiguities in the post-Newtonian expansion for binary systems, Phys. Rev. D 96 (2017) 024062 [1703.06433].
- [37] S. Foffa, R. A. Porto, I. Rothstein and R. Sturani, Conservative dynamics of binary systems to fourth Post-Newtonian order in the EFT approach II: Renormalized Lagrangian, Phys. Rev. D 100 (2019) 024048 [1903.05118].
- [38] S. Foffa, P. Mastrolia, R. Sturani, C. Sturm and W. J. Torres Bobadilla, *Static two-body potential at fifth post-Newtonian order*, *Phys. Rev. Lett.* **122** (2019) 241605 [1902.10571].

- [39] J. Blümlein, A. Maier and P. Marquard, Five-Loop Static Contribution to the Gravitational Interaction Potential of Two Point Masses, Phys. Lett. B 800 (2020) 135100 [1902.11180].
- [40] L. Bernard, L. Blanchet and D. Trestini, Gravitational waves in scalar-tensor theory to one-and-a-half post-Newtonian order, JCAP 08 (2022) 008 [2201.10924].
- [41] X. Zhang, T. Liu and W. Zhao, Gravitational radiation from compact binary systems in screened modified gravity, Phys. Rev. D 95 (2017) 104027 [1702.08752].
- [42] M. Quartin, S. Tsujikawa, L. Amendola and R. Sturani, Constraining Horndeski theory with gravitational waves from coalescing binaries, JCAP 08 (2023) 049 [2304.02535].
- [43] A. Chowdhuri and A. Bhattacharyya, Study of eccentric binaries in horndeski gravity, Phys. Rev. D 106 (2022) 064046.
- [44] L. De Vittori, A. Gopakumar, A. Gupta and P. Jetzer, Gravitational waves from spinning compact binaries in hyperbolic orbits, Phys. Rev. D 90 (2014) 124066 [1410.6311].
- [45] J. García-Bellido and S. Nesseris, Gravitational wave energy emission and detection rates of Primordial Black Hole hyperbolic encounters, Phys. Dark Univ. 21 (2018) 61 [1711.09702].
- [46] L. De Vittori, P. Jetzer and A. Klein, Gravitational wave energy spectrum of hyperbolic encounters, Phys. Rev. D 86 (2012) 044017 [1207.5359].
- [47] N. Dai, Y. Gong, T. Jiang and D. Liang, Intermediate mass-ratio inspirals with dark matter minispikes, Phys. Rev. D 106 (2022) 064003 [2111.13514].
- [48] A. Chowdhuri, R. K. Singh, K. Kangsabanik and A. Bhattacharyya, *Gravitational radiation from hyperbolic encounters in the presence of dark matter*, 2306.11787.
- [49] M. Levi, Binary dynamics from spin1-spin2 coupling at fourth post-Newtonian order, Phys. Rev. D 85 (2012) 064043 [1107.4322].
- [50] M. Levi and J. Steinhoff, Next-to-next-to-leading order gravitational spin-squared potential via the effective field theory for spinning objects in the post-Newtonian scheme, JCAP 01 (2016) 008 [1506.05794].
- [51] N. T. Maia, C. R. Galley, A. K. Leibovich and R. A. Porto, Radiation reaction for spinning bodies in effective field theory I: Spin-orbit effects, Phys. Rev. D 96 (2017) 084064 [1705.07934].
- [52] M. K. Mandal, P. Mastrolia, R. Patil and J. Steinhoff, Gravitational quadratic-in-spin Hamiltonian at NNNLO in the post-Newtonian framework, JHEP 07 (2023) 128 [2210.09176].

- [53] A. Bhattacharyya, S. Ghosh and S. Pal, Worldline effective field theory of inspiralling black hole binaries in presence of dark photon and axionic dark matter, JHEP 08 (2023) 207 [2305.15473].
- [54] R. F. Diedrichs, D. Schmitt and L. Sagunski, Binary Systems in Massive Scalar-Tensor Theories: Next-to-Leading Order Gravitational Waveform from Effective Field Theory, 2311.04274.
- [55] N. A. Collins and S. A. Hughes, Towards a formalism for mapping the space-times of massive compact objects: Bumpy black holes and their orbits, Phys. Rev. D 69 (2004) 124022 [gr-qc/0402063].
- [56] K. Glampedakis and S. Babak, Mapping spacetimes with LISA: Inspiral of a test-body in a 'quasi-Kerr' field, Class. Quant. Grav. 23 (2006) 4167 [gr-qc/0510057].
- [57] S. J. Vigeland and S. A. Hughes, Spacetime and orbits of bumpy black holes, Phys. Rev. D 81 (2010) 024030.
- [58] S. Vigeland, N. Yunes and L. C. Stein, Bumpy black holes in alternative theories of gravity, Phys. Rev. D 83 (2011) 104027.
- [59] D. Psaltis, Probes and Tests of Strong-Field Gravity with Observations in the Electromagnetic Spectrum, Living Rev. Rel. 11 (2008) 9 [0806.1531].
- [60] C. M. Will, The Confrontation between general relativity and experiment, Living Rev. Rel. 9 (2006) 3 [gr-qc/0510072].
- [61] T. Johannsen, Systematic study of event horizons and pathologies of parametrically deformed kerr spacetimes, Phys. Rev. D 87 (2013) 124017.
- [62] T. Johannsen and D. Psaltis, Testing the no-hair theorem with observations in the electromagnetic spectrum. i. properties of a quasi-kerr spacetime, The Astrophysical Journal 716 (2010) 187.
- [63] T. Johannsen and D. Psaltis, Testing the no-hair theorem with observations in the electromagnetic spectrum. ii. black hole images, The Astrophysical Journal 718 (2010) 446.
- [64] T. Johannsen and D. Psaltis, Testing the no-hair theorem with observations in the electromagnetic spectrum. iii. quasi-periodic variability, The Astrophysical Journal 726 (2010) 11.
- [65] T. Johannsen and D. Psaltis, Metric for rapidly spinning black holes suitable for strong-field tests of the no-hair theorem, Phys. Rev. D 83 (2011) 124015.

- [66] C. Bambi, Testing the Nature of Astrophysical Black Hole Candidates, Springer Proc. Phys. 145 (2014) 81.
- [67] N. Tsukamoto, Z. Li and C. Bambi, Constraining the spin and the deformation parameters from the black hole shadow, JCAP 06 (2014) 043 [1403.0371].
- [68] C. Bambi and E. Barausse, Constraining the quadrupole moment of stellar-mass black-hole candidates with the continuum fitting method, Astrophys. J. **731** (2011) 121 [1012.2007].
- [69] D. Psaltis and T. Johannsen, A Ray-tracing Algorithm for Spinning Compact Object Spacetimes with Arbitrary Quadrupole Moments. I. Quasi-Kerr Black Holes, apj 745 (2012) 1 [1011.4078].
- [70] F. D. Ryan, Effect of gravitational radiation reaction on nonequatorial orbits around a Kerr black hole, Phys. Rev. D 53 (1996) 3064 [gr-qc/9511062].
- [71] C. Li and G. Lovelace, Generalization of ryan's theorem: Probing tidal coupling with gravitational waves from nearly circular, nearly equatorial, extreme-mass-ratio inspirals, Phys. Rev. D 77 (2008) 064022.
- [72] L. Barack and C. Cutler, Lisa capture sources: Approximate waveforms, signal-to-noise ratios, and parameter estimation accuracy, Phys. Rev. D 69 (2004) 082005.
- [73] J. Brink, Spacetime encodings. ii. pictures of integrability, Phys. Rev. D 78 (2008) 102002.
- [74] J. Gair and N. Yunes, Approximate waveforms for extreme-mass-ratio inspirals in modified gravity spacetimes, Phys. Rev. D 84 (2011) 064016.
- [75] P. Amaro-Seoane, H. Audley, S. Babak, J. Baker, E. Barausse, P. Bender et al., Laser Interferometer Space Antenna, arXiv e-prints (2017) arXiv:1702.00786 [1702.00786].
- [76] S. Babak, J. Gair, A. Sesana, E. Barausse, C. F. Sopuerta, C. P. L. Berry et al., Science with the space-based interferometer LISA. V: Extreme mass-ratio inspirals, Phys. Rev. D 95 (2017) 103012 [1703.09722].
- [77] P. Amaro-Seoane, J. R. Gair, M. Freitag, M. Coleman Miller, I. Mandel, C. J. Cutler et al., Astrophysics, detection and science applications of intermediate- and extreme mass-ratio inspirals, Class. Quant. Grav. 24 (2007) R113 [astro-ph/0703495].
- [78] T. Hinderer and E. E. Flanagan, Two timescale analysis of extreme mass ratio inspirals in Kerr. I. Orbital Motion, Phys. Rev. D 78 (2008) 064028 [0805.3337].
- [79] S. Drasco and S. A. Hughes, Gravitational wave snapshots of generic extreme mass ratio inspirals, Phys. Rev. D 73 (2006) 024027 [gr-qc/0509101].

- [80] M. Rahman, S. Kumar and A. Bhattacharyya, Gravitational wave from extreme mass-ratio inspirals as a probe of extra dimensions, JCAP 01 (2023) 046 [2212.01404].
- [81] M. Rahman and A. Bhattacharyya, Prospects for determining the nature of the secondaries of extreme mass-ratio inspirals using the spin-induced quadrupole deformation, 2112.13869.
- [82] A. Maselli, N. Franchini, L. Gualtieri, T. P. Sotiriou, S. Barsanti and P. Pani, Detecting fundamental fields with LISA observations of gravitational waves from extreme mass-ratio inspirals, Nature Astron. 6 (2022) 464 [2106.11325].
- [83] J. R. Gair, S. Babak, A. Sesana, P. Amaro-Seoane, E. Barausse, C. P. L. Berry et al., Prospects for observing extreme-mass-ratio inspirals with LISA, J. Phys. Conf. Ser. 840 (2017) 012021 [1704.00009].
- [84] LISA collaboration, New horizons for fundamental physics with LISA, Living Rev. Rel. 25 (2022) 4 [2205.01597].
- [85] L. V. Drummond, P. Lynch, A. G. Hanselman, D. R. Becker and S. A. Hughes, Extreme mass-ratio inspiral and waveforms for a spinning body into a Kerr black hole via osculating geodesics and near-identity transformations, 2310.08438.
- [86] K. Fransen and D. R. Mayerson, Detecting equatorial symmetry breaking with LISA, Phys. Rev. D 106 (2022) 064035 [2201.03569].
- [87] I. Bena and D. R. Mayerson, Multipole ratios: A new window into black holes, Phys. Rev. Lett. 125 (2020) 221602.
- [88] M. Bianchi, D. Consoli, A. Grillo, J. F. Morales, P. Pani and G. Raposo, Distinguishing fuzzballs from black holes through their multipolar structure, Phys. Rev. Lett. 125 (2020) 221601 [2007.01743].
- [89] M. Rahman, S. Kumar and A. Bhattacharyya, *Probing astrophysical environment with eccentric extreme mass-ratio inspirals*, 2306.14971.
- [90] K. Destounis and K. D. Kokkotas, Gravitational-wave glitches: Resonant islands and frequency jumps in nonintegrable extreme-mass-ratio inspirals, Phys. Rev. D 104 (2021) 064023.
- [91] E. E. Flanagan and T. Hinderer, Evolution of the Carter constant for inspirals into a black hole: Effect of the black hole quadrupole, Phys. Rev. D 75 (2007) 124007 [0704.0389].
- [92] T. Johannsen, Regular Black Hole Metric with Three Constants of Motion, Phys. Rev. D 88 (2013) 044002 [1501.02809].

- [93] S. Staelens, D. R. Mayerson, F. Bacchini, B. Ripperda and L. Küchler, Black hole photon rings beyond general relativity, Phys. Rev. D 107 (2023) 124026 [2303.02111].
- [94] Z. Carson and K. Yagi, Asymptotically flat, parameterized black hole metric preserving Kerr symmetries, Phys. Rev. D 101 (2020) 084030 [2002.01028].
- [95] V. Cardoso, P. Pani and J. Rico, On generic parametrizations of spinning black-hole geometries, Phys. Rev. D 89 (2014) 064007 [1401.0528].
- [96] K. Glampedakis, S. A. Hughes and D. Kennefick, Approximating the inspiral of test bodies into Kerr black holes, Phys. Rev. D 66 (2002) 064005 [gr-qc/0205033].
- [97] K. Glampedakis and D. Kennefick, Zoom and whirl: Eccentric equatorial orbits around spinning black holes and their evolution under gravitational radiation reaction, Phys. Rev. D 66 (2002) 044002 [gr-qc/0203086].
- [98] S. A. Hughes, Evolution of circular, nonequatorial orbits of kerr black holes due to gravitational-wave emission, Phys. Rev. D 61 (2000) 084004.
- [99] V. Skoupý and G. Lukes-Gerakopoulos, Spinning test body orbiting around a Kerr black hole: Eccentric equatorial orbits and their asymptotic gravitational-wave fluxes, Phys. Rev. D 103 (2021) 104045 [2102.04819].
- [100] V. Skoupý and G. Lukes-Gerakopoulos, Spinning test body orbiting around a kerr black hole: Eccentric equatorial orbits and their asymptotic gravitational-wave fluxes, Phys. Rev. D 103 (2021) 104045.
- [101] C. Cutler, D. Kennefick and E. Poisson, Gravitational radiation reaction for bound motion around a schwarzschild black hole, Phys. Rev. D 50 (1994) 3816.
- [102] P. A. Sundararajan, Transition from adiabatic inspiral to geodesic plunge for a compact object around a massive kerr black hole: Generic orbits, Phys. Rev. D 77 (2008) 124050.
- [103] S. A. Hughes, The Evolution of circular, nonequatorial orbits of Kerr black holes due to gravitational wave emission, Phys. Rev. D 61 (2000) 084004 [gr-qc/9910091].
- [104] F. D. Ryan, Effect of gravitational radiation reaction on circular orbits around a spinning black hole, Phys. Rev. D 52 (1995) R3159.
- [105] S. A. Hughes, N. Warburton, G. Khanna, A. J. K. Chua and M. L. Katz, Adiabatic waveforms for extreme mass-ratio inspirals via multivoice decomposition in time and frequency, Phys. Rev. D 103 (2021) 104014.

- [106] S. Isoyama, R. Fujita, A. J. K. Chua, H. Nakano, A. Pound and N. Sago, Adiabatic waveforms from extreme-mass-ratio inspirals: An analytical approach, Phys. Rev. Lett. 128 (2022) 231101.
- [107] P. C. Peters and J. Mathews, Gravitational radiation from point masses in a keplerian orbit, Phys. Rev. 131 (1963) 435.
- [108] P. C. Peters, Gravitational radiation and the motion of two point masses, Phys. Rev. 136 (1964) B1224.
- [109] S. A. Hughes, N. Warburton, G. Khanna, A. J. K. Chua and M. L. Katz, Adiabatic waveforms for extreme mass-ratio inspirals via multivoice decomposition in time and frequency, Phys. Rev. D 103 (2021) 104014 [2102.02713].
- [110] N. Dai, Y. Gong, Y. Zhao and T. Jiang, Extreme mass ratio inspirals in galaxies with dark matter halos, 2301.05088.
- [111] S. Barsanti, N. Franchini, L. Gualtieri, A. Maselli and T. P. Sotiriou, Extreme mass-ratio inspirals as probes of scalar fields: Eccentric equatorial orbits around Kerr black holes, Phys. Rev. D 106 (2022) 044029 [2203.05003].
- [112] B. Moore, M. Favata, K. G. Arun and C. K. Mishra, Gravitational-wave phasing for low-eccentricity inspiralling compact binaries to 3PN order, Phys. Rev. D 93 (2016) 124061 [1605.00304].
- [113] LIGO SCIENTIFIC, VIRGO, KAGRA collaboration, Tests of General Relativity with GWTC-3, 2112.06861.
- [114] B. Bonga, H. Yang and S. A. Hughes, *Tidal resonance in extreme mass-ratio inspirals*, *Phys. Rev. Lett.* **123** (2019) 101103.
- [115] K. Glampedakis and S. Babak, Mapping spacetimes with LISA: inspiral of a test body in a 'quasi-kerr' field, Classical and Quantum Gravity 23 (2006) 4167.
- [116] K. Glampedakis, Extreme mass ratio inspirals: Lisa's unique probe of black hole gravity, Classical and Quantum Gravity 22 (2005) S605.
- [117] T. Johannsen, Regular black hole metric with three constants of motion, Phys. Rev. D 88 (2013) 044002.
- [118] D. Li, P. Wagle, Y. Chen and N. Yunes, Perturbations of Spinning Black Holes beyond General Relativity: Modified Teukolsky Equation, Phys. Rev. X 13 (2023) 021029 [2206.10652].

- [119] A. Pound and B. Wardell, Black hole perturbation theory and gravitational self-force, 2101.04592.
- [120] M. Vallisneri, Use and abuse of the Fisher information matrix in the assessment of gravitational-wave parameter-estimation prospects, Phys. Rev. D 77 (2008) 042001 [gr-qc/0703086].
- [121] C. W. Misner, K. S. Thorne and J. A. Wheeler, *Gravitation*. W. H. Freeman, San Francisco, 1973.
- [122] T. Hinderer and E. E. Flanagan, Two-timescale analysis of extreme mass ratio inspirals in kerr spacetime: Orbital motion, Phys. Rev. D 78 (2008) 064028.
- [123] S. Mukherjee and S. Chakraborty, Transition from inspiral to plunge for braneworld EMRI, Class. Quant. Grav. 40 (2023) 145013 [2212.07018].